

RICE UNIVERSITY

Multimodal Optical Imaging for Detection of Cervical Neoplasia

by

Tefo Caddrouse Bubi

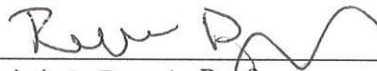
A THESIS SUBMITTED
IN PARTIAL FULFILLMENT OF THE
REQUIREMENTS FOR THE DEGREE

Doctor of Philosophy

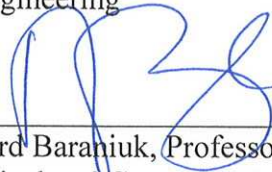
APPROVED, THESIS COMMITTEE:



Rebecca Richards-Kortum, Stanley C. Moore Professor
Bioengineering



Rebekah A. Drezek, Professor
Bioengineering



Richard Baraniuk, Professor
Electrical and Computer Engineering

HOUSTON, TEXAS
APRIL, 2013

ABSTRACT

Multimodal Optical Imaging for Detection of Cervical Neoplasia

by

Tefo Caddrouse Bubi

Despite being the most preventable cancer, cervical cancer remains the third leading cause of cancer death worldwide. Over 85% of cervical cancer incidence and mortality occurs in low-resource countries where screening programs for early detection are either inadequate or unavailable. In the developed world, where screening programs are well organized, incidence and mortality rates are greatly reduced. Recent advances in optical imaging have the potential to enable cervical cancer screening at the point-of-care, even in the hands of less experienced providers. High performance optical imaging systems can be constructed at relatively low cost, and image analysis can be automated; thus, these technologies may provide a way to bridge the gap to cervical cancer screening for developing countries. This work focuses on the design, construction, and clinical testing of a novel multimodal optical imaging (combination of wide-field imaging and high-resolution) for early detection of cervical neoplasia.

The Multimodal Digital Imager (MDI) acquires *in vivo* images of cervical tissue in fluorescence, narrow band reflectance, and orthogonal polarized reflectance modes using multiple illumination wavelengths. The High Resolution Microendoscope (HRME) was used to interrogate

clinically suspicious areas with subcellular spatial resolution, revealing changes in nuclear to cytoplasmic area ratio.

In vivo image data from the wide-field system was combined with image data from a high-resolution microendoscope (HRME) in order to test the effectiveness of the multimodal optical imaging in discriminating between cervical neoplasia and non-neoplastic. Multimodal optical imaging coupled with computer aided diagnostic achieved a sensitivity of 82% and specificity of 85% for discriminating cervical neoplastic from non-neoplastic

This work has demonstrated that multimodal optical imaging; combination of wide-field and high-resolution optical imaging of the cervix can assist in the detection of cervical neoplasia and can be implemented effectively in a low-resource setting.

DEDICATION

To my Mother, Esther Khutsafalo Bubi.

Acknowledgements

First and foremost, I would like to thank my advisor, Dr. Rebecca Richards-Kortum, for her professional guidance over the past five years. The opportunity you have afforded me will not only personally benefit, but my country, Botswana as a whole. Thank you for been there for me at all times.

Many thanks to the other members of my committee: Dr. Rebekah Drezek, and Dr Richard Baraniuk, for their advice and support. I was honored to have you in my committee.

I would also like to thank the collaborators that I have worked with so closely: Dr. Doreen Ramogola-Masire and Dr Kayembe in Botswana. Who worked tirelessly to make this work possible.

I would like to thank current and former members of the Kortum Lab for their help and support, including Dr. Mark Pierce, Dr Nadhi Thekkek, Dongsuk Shin, Vivian Mack, and Mary Kate Quinn; and especially John Wright who has helped me with the research but most importantly, for been a friend over the past five years.

I could not have done it without the support of my wife; Omphile who has been there for me every step of the way. Thank you so much to my boys; Thero and Bakang for understanding when I came home late, when I missed their birthday celebrations, or when I wasn't able to take them to the soccer field on some Saturdays.

TABLE OF CONTENTS

Abstract	1
Dedication.....	iv
Acknowledgements.....	v
Table of Contents.....	vi
CHAPTER 1: Introduction	1
1.1 Overview.....	1
1.2 Specific Aims.....	2
1.3 Summary.....	3
CHAPTER 2: Background	5
2.1 Motivation and Significance.....	5
2.2 Cervix.....	8
2.2.1 Normal Anatomy and histology.....	8
2.2.2 The Dysplasia to Carcinoma Sequence.....	10
2.3 Current and emerging methods of Early Detection and Prevention.....	12
2.3.1 Resource Intensive Regions.....	12
2.3.1.1 Pap smear and Colposcopy.....	12
2.3.1.2 HPV Vaccines.....	14
2.3.2 Resource limited regions	
2.3.2.1 HPV-DNA and Visual Inspection with acetic Acid.....	15
2.4 Optical Imaging Systems.....	17

2.4.1 Role of optics in cancer.....	17
2.4.2 Wide-field Imaging Systems.....	19
2.4.3 High-Resolution Imaging Systems.....	21
2.5 Proflavine.....	23
CHAPTER 3: High-Resolution Microendoscope For The Detection Of Cervical Neoplasia In Low-Resource Settings.....	25
3.1 Introduction.....	26
3.2 Materials and Methods.....	29
3.2.1 Instrumentation.....	29
3.2.2 Clinical Measurements.....	30
3.2.3 Data Analysis.....	31
3.2.4 Ethics Statement.....	32
3.3 Results.....	33
3.4 Discussion.....	38
CHAPTER 4: HRME Validation Paper.....	41
4.1 Introduction.....	41
4.2 Materials And Methods.....	43
4.2.1 Study Population.....	43
4.2.2 Data analysis.....	45
4.3 Results.....	47
4.4 Discussion.....	48

CHAPTER 5: Multimodal Digital Imager For The Detection Of Cervical

Neoplasia In Low-Resource Settings.....52

5.1 Introduction.....52

5.2 Materials and Methods.....53

5.2.1 Instrumentation.....5.3

5.2.2 In vivo pilot study.....56

5.2.3 Data processing.....58

5.3 Results.....60

5.4 Discussion.....62

CHAPTER 6: Wide-Field Multimodal Imaging And High-Resolution

Microendoscope Imaging For Detection Of Cervical Neoplasia.....66

6.1 Introduction.....66

6.2 Materials and Methods.....68

6.2.1 Study population.....68

6.2.2 Imaging systems.....69

6.2.3 Study procedure.....69

6.2.4 Image Analysis – WF Imaging.....70

6.2.5 Image Analysis – High-resolution Imaging (HRME).....71

6.2.6 Image Classification.....72

6.3 Results.....73

6.3.1 Wide-field and HRME imaging.....74

6.3.2 Classification Performance.....75

6.4 Discussion.....78

CHAPTER 7: Conclusion.....81

References.....85

1. INTRODUCTION

1.1 Overview

The main objective of this research is to evaluate whether multimodal optical imaging (a combination of wide-field and high-resolution optical imaging) of the cervix can assist clinicians in detecting dysplastic (precancerous) areas, in a bid to provide screening alternatives to the low-resourced world.

It is important to detect and treat precancerous lesions of the cervix before they develop into cancer. Cervical precancers are typically associated with architectural, morphologic and molecular changes that are normally detected via cytology and/or histology.

Recent advances in fiber optics, optical detectors, and computer-aided image analysis have given rise to new optical imaging systems with the potential to image cells or tissue, revealing architectural and morphologic disease characteristics without the need for tissue removal. Optical imaging systems are able to obtain and display both wide-field and high-resolution images of epithelial tissues in real-time. Wide-field systems enable relatively large fields of view (50-100 mm) to be visualized at moderate resolution under conventional white-light illumination, as well as in fluorescence and polarized light modes. Advances in wide-field narrow-band reflectance imaging can also be utilized to enhance vascular contrast. High-resolution optical imaging techniques have been used to observe morphologic and architectural changes in cells that indicate neoplastic transformation. Such indicators are changes in the size and internal structure of the nucleus, the disorganization of cells, pleomorphism, and other cellular changes that require imaging with spatial resolution on the order of a few microns. Fluorescent contrast agents are also available to enhance visualization of suspicious lesions by increasing the signal to background ratio.

A combination of these advances was explored to aid in the detection of cervical intraepithelial neoplasia (CIN). Wide-field imaging was used to rapidly image the entire cervix and identify regions which are suspicious for neoplasia with high sensitivity, while high-resolution imaging used to interrogate suspicious regions identified in wide-field imaging with high spatial resolution, confirming the presence or absence of neoplasia with high specificity. In vivo studies were performed to determine the imaging techniques and parameters which maximize diagnostic performance. Finally, data acquired in vivo were used to develop and evaluate image analysis algorithms acquired using these optimal parameters.

1.2 Objective and Specific Aims

Specific Aim 1: A multimodal wide-field optical imaging system termed the Multimodal Digital Imager (MDI) was designed, constructed and its performance characterized. The MDI is capable of narrowband green reflectance, cross-polarized reflectance, and fluorescence imaging across the entire field of view of the cervix, with moderate spatial resolution.

Specific Aim 2: An in vivo pilot study involving 26 patients in Gaborone, Botswana was conducted using the MDI and a high-resolution micro-endoscope (HRME) previously developed in our lab. The imaging parameters of the systems were optimized, and the ability of each individual system to discriminate cervical cancer from normal tissue relative to the gold standard of histopathology established. Data from these 26 patients were used to optimize image analysis parameters, and served as a training set to develop and evaluate automated, quantitative image processing algorithms.

Specific Aim 3: A larger study involving 60 patients in a high prevalence population in Botswana was conducted. Images were obtained with the wide-field system and the high-resolution microendoscope. Data were analyzed using algorithms optimized in the training set to determine the sensitivity and specificity of the wide-field and high-resolution optical imaging.

1.3 Summary

This dissertation describes the development of novel, multimodal optical imaging devices for diagnosis of cervical cancer that can be implemented as diagnostic aids in high-prevalence patient populations. Optical modalities and conditions that could provide improved information on the presence of cervical lesions in vivo were explored using these devices. Previous studies investigated the ability of some individual optical imaging devices to identify lesions, however, this is the first work to combine multiple modalities including multimodal wide-field and high-resolution imaging of the cervix, with the intention to improve detection accuracy.

The dissertation is organized as follows: Chapter 2 presents relevant background information on cervical cancer and premalignant lesions. Current methods for detection and diagnosis are discussed. The role of optics in cancer is also discussed together with current optical diagnostic techniques. Chapter 3 reports initial results of in vivo pilot study on the cervix using the high-resolution microendoscopy system. Quantitative image analysis algorithms were developed that demonstrate the ability of the microendoscope to distinguish between neoplastic and non-neoplastic tissue in human cervical squamous epithelium. To demonstrate the ability of the microendoscope system to give consistent results in detecting neoplastic lesions in the cervix, Chapter 4 presents results from a larger study. These results are used as a validation set to test the algorithms developed in chapter 3. Chapter 5 presents the design and performance

characteristics of the multimodal digital imager (MDI). Initial results of a study on the MDI system including in vivo imaging of the cervix are presented. Chapter 6 seeks to investigate the ability of integrating the microendoscope system with other wide-field systems. Data from the microendoscope system were combined with data from the wide-field system in order to maximize sensitivity and specificity. Chapter 7 summarizes and discusses the important findings and implications of this dissertation.

2. BACKGROUND

2.1 Motivation and Significance

Cervical cancer is the third most common type of cancer in women worldwide. In 2008, 530,000 new cases and 275,000 deaths from cervical cancer were estimated [1]. Over 85% of cervical cancer incidence and mortality occur in developing countries where screening programs for early detection are either

inadequate or unavailable [1].

It is estimated that this number will be 90% by 2020 if no major interventions are carried out now [2, 3].

Cervical cancer incidence and mortality rates are highest in sub-Saharan Africa where incidence rates are nearly 7 times higher than that of North America, and mortality rates are 15 times as high [2].

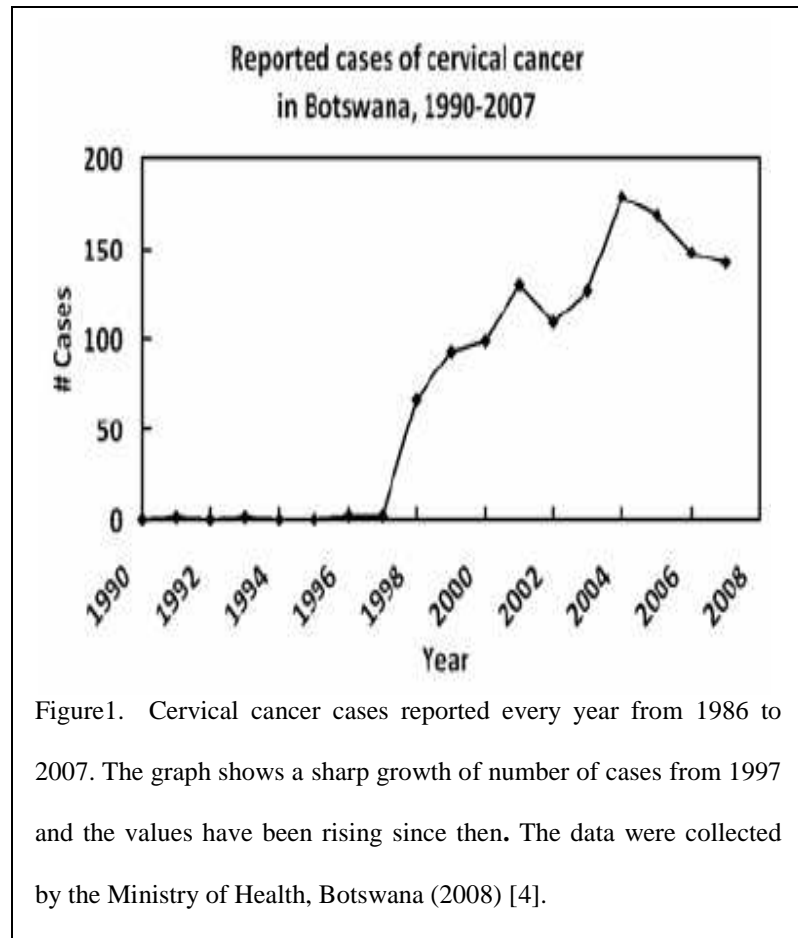


Figure1. Cervical cancer cases reported every year from 1986 to 2007. The graph shows a sharp growth of number of cases from 1997 and the values have been rising since then. The data were collected by the Ministry of Health, Botswana (2008) [4].

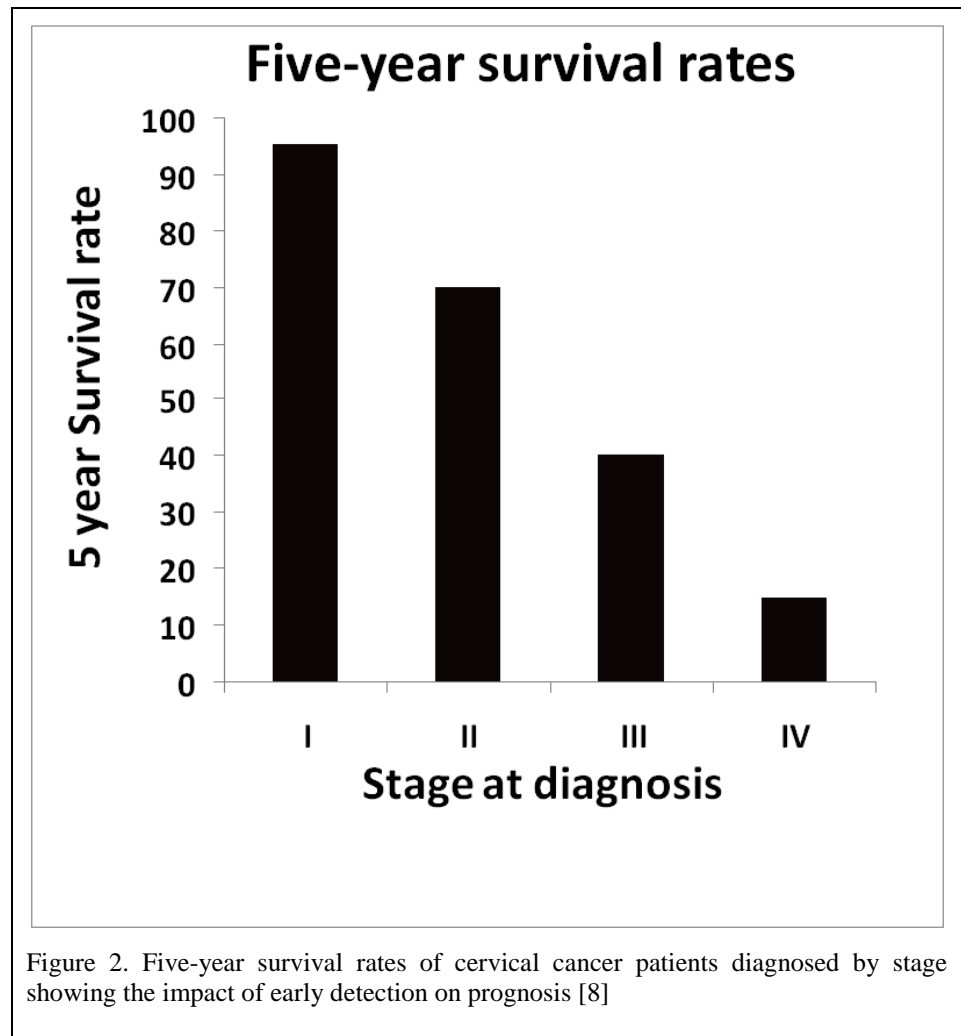
In developed countries, organized screening tests such as the Papanicolaou smear have enabled precancerous lesions to be diagnosed and treated early, subsequently reducing new cervical cancer cases and mortality rates. However, to be effective, these screening programs require relatively high-level infrastructure and well-trained personnel.

Cervical cancer affects mostly young women in developing countries who are in their most productive years. Most of these patients have this insidious disease due to late detection, when treatment is particularly difficult. Late detection is due to a lack of or inadequate screening tools/programs because of financial and personnel constraints.

In Botswana, where we carried out research, cervical cancer accounted for over 24% of all cancers among

women in 2007 [4].

Botswana has high HIV/AIDS incidence rates and with studies showing HIV correlation to HPV and cervical neoplasia [5], it is not surprising to see an increase of cervical cancer during the HIV era. Figure 1 shows the growth in the number of reported cases of



cervical cancer in Botswana over the past 21 years [4]. Due to rising incidence, improving early diagnosis at the point-of-care is particularly important in this setting.

Cervical cancer is almost 100% curable when detected early [6]. The 5-year survival rates for cervical cancer are strongly dependent on the stage of diagnosis. Figure 2 shows the correlation between survival rates and stage at diagnosis.

Current screening and diagnosis of cervical precancer involves collection of cells from the cervix by a cytology test (Pap smear). The 70% decrease in the incidence of cervical cancer in the US has been credited in a large part to the widespread use of the Papanicolaou smear [7]. An abnormal Pap smear is followed by colposcopy, an optically based technique developed in the early 1900's [6]. A colposcope is a low-power microscope that illuminates and magnifies the cervix, to help take directed biopsies of the abnormal appearing tissue. Acetic acid and Lugol's iodine have been used with the colposcope to improve optical contrast. Because of the low specificity (48%) of colposcopy, a biopsy is required to confirm disease [8]. This low specificity leads to over-diagnosis of low-grade lesions, hence the need for biopsy confirmation.

Of late, there have been significant improvements in colposcopy to enhance contrast. Green filters have been incorporated to further enhance vascular contrast, highlighting suspicious regions. Digital colposcopes have also been developed to collect digital images which can be analyzed visually or using image analysis algorithms.

In developed countries the incidence and mortality rates of cervical cancer have been greatly decreased due to this approach. Further reduction is anticipated with the latest HPV vaccine developments, since about 70% of cervical cancer is caused by the high-risk HPV infections covered by available vaccines.

The necessity of biopsy to confirm colposcopic impression leads to the need for extensive infrastructure, personnel and economic resources. This expensive approach is not possible to implement in developing countries, and, as a result, a majority of women die from the disease

due to diagnosis at late stage. Early cervical cancer detection methods that are accurate but less expensive and that allow immediate treatment and prevention methods are crucial for low-resourced countries.

2.2 Cervix

2.2.1 Normal Anatomy and histology

The cervix is the lower part of the uterus on the vaginal side. It is also referred to as “neck of the uterus”. The cervix is about 3-5cm in diameter but varies depending on the woman’s age and hormonal status. Figure 3 shows a diagram of the lower female genital tract and shows the location of the cervix [9]. The cervix has four main parts: Ectocervix; the portion projecting into the vagina, External os; opening of the ectocervix, Endocervix; the canal of the cervix

connecting the external os to the internal os, Internal os; the opening of the cervix into the uterine cavity [10, 11].

The cervix is lined by two types of epithelium. The ectocervix is composed of non-keratinized stratified squamous epithelium while

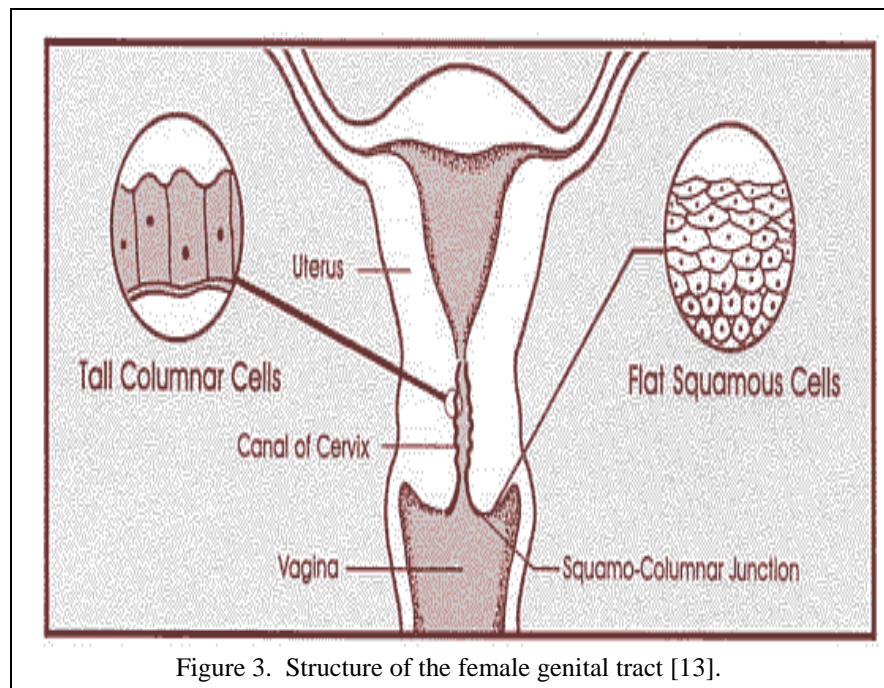


Figure 3. Structure of the female genital tract [13].

the endocervix is composed of simple columnar epithelium [9 - 12]. The fact that there are two types of epithelium present is important because their optical properties are different.

The squamous tissue of the ectocervix consists of three distinct epithelial layers; the superficial top layer that consists of mature cells, the intermediate layer that consists of maturing cells, and the basal layer that consists of metabolically active, mitotic cells that regenerate the epithelium. Mature squamous epithelium contains abundant glycogen, hence changes color after application of Lugol's iodine. The female hormone, estrogen is responsible for the maturation of the squamous epithelium.

The columnar/glandular tissue of the endocervix consists mainly of columnar cells with glandular structures for mucous secretion. It is composed of a single layer of tall cells. It is in the columnar epithelium where endocervical crypts form. The columnar epithelium does not contain glycogen. Due to the absence of glycogen, columnar epithelium does not change color after application of Lugol's iodine. This is one way to distinguish squamous and columnar epithelium.

The area at the border of the squamous and columnar tissue is called the transformation zone. There are normal physiological changes that cause metaplasia in the transformation zone including menopause, puberty, and the menstrual cycle. Metaplasia is the replacement of the columnar epithelium by squamous epithelium. The environment of the ectocervix is different from that of the endocervix, the former being slightly acidic. When the endocervix is exposed to the acidic conditions of the vagina it will undergo metaplasia. Metaplasia is a normal, non-cancerous process that every woman undergoes in her life [13 - 15].

Some human papillomavirus (HPV) types insult the squamous metaplastic region resulting in nuclear and cytoplasmic abnormalities [10]. If the infection is not cleared by the patient's immune system, this benign condition is capable of becoming dysplastic and then cancerous.

Close attention should be given to the transformation zone because metaplasia occurs here and it has a higher risk of becoming dysplastic and then cancerous.

2.2.2 The Dysplasia to Carcinoma Sequence

Invasive cervical cancers can be prevented since they are preceded by a long phase of preinvasive disease (dysplasia). Cervical dysplasia refers to abnormal cell growth of the cervix. Cervical dysplasia is caused by infection of the cervix with the human papillomavirus (HPV) infection, which is transmitted through sexual contact. HPV 16 and 18 have been associated with about 70% of severe dysplasia and cervical cancer. HPV 6 and 11 are strongly associated with genital warts. The

immune system

attempts to clear these

infections, and about

90% are cleared within

two years.

Cervical dysplasia is

divided into low-grade

squamous

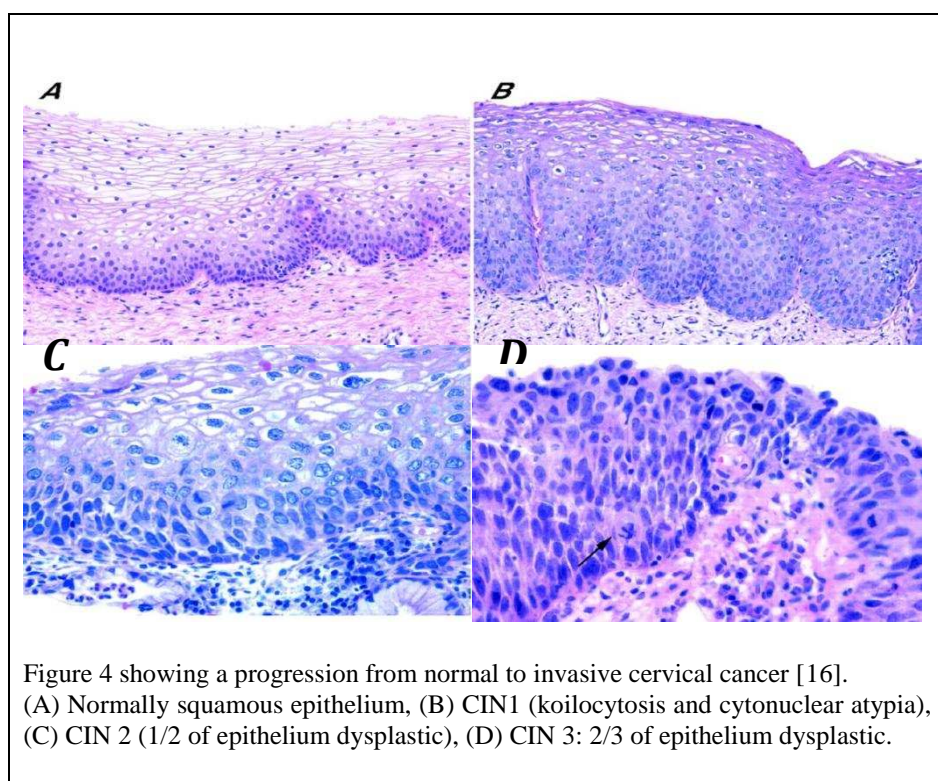
intraepithelial lesions

(LGSIL) and high-

grade squamous intraepithelial lesions (HGSIL). LGSIL includes koilocytic atypia and CIN 1,

while HGSIL includes CIN 2 & 3. CIN refers to cervical intraepithelial neoplasia. In CIN 1, the

lower 1/3 of the epithelium includes precancerous cells. In CIN 2, the lower 1/2 of the epithelium



includes precancerous cells, and in CIN 3, the lower 2/3 of the epithelium includes precancerous cells. Figure 4 [16] shows the progression from normal epithelium to HGSIL. In CIN 1 there are just a few abnormal cells growing in the basal layer, while in CIN 2, about half of the cells are abnormal beginning in the basal layer, and in CIN 3 more than two-thirds of the cells are abnormal. When the entire epithelium is filled with precancerous cells which have not yet spread below the surface, the lesion is referred to as carcinoma-in-situ (CIS) [17]. When carcinoma in situ is left untreated, it can often progress to invasive cervical cancer, where the neoplastic cells invade the tissue underlying the basement membrane. There are two main types of invasive cervical cancer: squamous cell cancer arising from the squamous epithelium that covers the ectocervix, and adenocarcinoma arising from the glandular cells of the endocervical canal. About 90% of cervical cancers are squamous cell cancers. Adenocarcinomas account for 10% of cervical cancer but are becoming more common in women born in the last two and three decades [18].

2.3 Current and emerging methods of Early Detection and Prevention

There is clear disparity between the incidence and mortality of cervical cancer in developed and developing countries. These disparities arise primarily as a result of the resources available for screening and early detection programs in these areas. Developed countries have organized screening programs to detect and treat cervical cancer and its precancers. However, for proper implementation, these programs require extensive infrastructure, personnel and economic resources. Unfortunately, these resources are not readily available in developing countries. Researchers have embarked on finding screening alternatives adoptable in developing nations.

2.3.1 Resource Intensive Regions

2.3.1.1 Pap smear and Colposcopy

In developed countries the current paradigm for screening and diagnosis of cervical precancer involves collection of cells from the cervix by a cytology test (Pap smear). Any abnormal Pap smear is followed by an optically based technique, called colposcopy [6], first described by Hinselmann in the early 1900's. A colposcope is a low-power microscope that illuminates and magnifies the cervix, helping the colposcopist to visually discriminate normal from abnormal tissue and to take directed biopsies of abnormal tissue. Acetic acid and Lugol's iodine have been used with the colposcope to improve optical contrast. Upon application of 3-5% acetic acid, suspicious areas turn white; the phenomenon is referred to as "acetowhitening". This is believed to come about because of increased cellular protein and increased nuclear density [8, 19, and 20]. Lugol's iodine is glycophilic that is the epithelium containing glycogen takes up the iodine. Normal squamous epithelium contains glycogen hence is expected to take up iodine, staining dark brown or black, while columnar epithelium contains no glycogen and hence remains

unstained. CIN and cancer contain less or no glycogen and don't stain upon application of iodine. Any areas in the squamous epithelium that remain unstained after application of iodine are therefore suspected to be dysplastic or cancerous. The colposcope is used to identify which regions of tissue should be biopsied. Biopsied tissue is then sent to a pathologist for further histologic analysis. Following confirmation of presence disease by histopathology, precancerous lesions are effectively treated using outpatient ablative or excisional techniques such as cryotherapy or loop electrosurgical excision procedure (LEEP), preventing the development of cervical cancer.

This process of evaluation is not only expensive but also time consuming. In developing countries, it can often require between 3 weeks to 6 months to obtain biopsy results, due to shortages in the number of trained pathologists. This can result in poor patient follow up, as patients must often travel long distances to receive medical attention. Also the three steps of this process are largely subjective, involving three different clinician's assessment of three distinct pathological entities.

The Pap smear test has an average sensitivity and specificity of 73% and 63% [21]. The low sensitivity leads to missed high-grade lesions and low specificity to over-diagnosed low-grade lesions. There is therefore the need for colposcopy. However, even in the hands of an expert, a low specificity of about 48% has been reported when differentiating abnormal from normal tissues [8]. A biopsy is therefore required to confirm disease, exposing patients to unnecessary biopsies. Biopsies significantly increase the cost; over US\$6B are spent annually in the United States to evaluate and treat atypias [22].

2.3.1.2 HPV Vaccines

Cervical cancer is caused by high-risk types of human papillomavirus (HPV). DNA from HPV 16 & 18 is found in more than 70% of squamous cell carcinomas [23, 24, and 25]. HPV is transmitted through sexual intercourse and approximately 70% of cervical cancers are caused by HPV 16 & 18 [24- 28]. Two vaccines, Gardasil and Cervarix, have recently been developed to protect against HPV 16 & 18. Gardasil has been studied in over 27,000 women in 33 countries and has received FDA licensing and is available in more than 60 countries [29]. The efficacy results for prevention of HPV 16 & 18 infection have been consistent in all these countries. Vaccines to prevent HPV infection that have been developed may further reduce the incidence of cervical cancer in countries where vaccines are available [28]. However, the high cost of vaccines, cultural acceptability, public support and political or logistical barriers could delay implementation of these vaccines in many developing countries [30]. In USA, the three-dose vaccine costs about \$360 [31]; this is a major barrier to implement in countries with a gross domestic product of less than \$1,000 per capita. The vaccine is effective only against HPV 16 & 18, which account for about 70% of cervical cancers, therefore routine cervical cancer screening is still essential even for vaccinated women to catch the other 30% cervical cancers not covered by the vaccinations.

2.3.2 Resource limited regions

2.3.2.1 HPV-DNA testing and Visual Inspection with acetic Acid (VIA)

Due to costs associated with cervical cancer surveillance methods used in developed countries it is almost impossible to use the same approach in developing countries.

Efforts have been made to provide cost-effective screening/diagnosis tools, such as DNA testing for HPV and simple visual inspection with acetic acid (VIA) in resource limited regions. HPV DNA testing has shown promising results when complementing cytology in primary screening [32, 33]. Goldie et al evaluated a variety of cervical cancer screening techniques for cost effectiveness in five different countries; India, Kenya, Peru, South Africa and Thailand. The HPV DNA test showed promising results with sensitivity and specificity of HPV DNA varying from 65% to 95% and 70% to 96% respectively [7]. In another study involving 2944 previously unscreened South African women, Hybrid Capture I (HCI) and Hybrid Capture II (HCII) assays [34] were evaluated. The HCI was found to have the same sensitivity as the better specificity than either the HCI or HCII assay. These results suggest that HPV testing may be considered for primary cervical cancer screening in low-resource settings since it is easier to implement than cytology screening. Although it is anticipated that HPV DNA testing may reduce costs that are associated with unnecessary colposcopy, the current available HPV tests are still relatively expensive to be fully implemented in low-resource settings, there is need for laboratory infrastructure for processing. Also, currently available HPV tests require six hours to produce a result, resulting in multiple clinic visits for screening and treatment.

More recently, rapid HPV test (careHPV) has been developed and promises to offer potential solutions to the limitations associated to the currently available HPV tests [35]. The test does not need a laboratory; it can be run in rural areas and mobile clinics. Single clinic visit may

be realized as test results are available within two and half hours. Qiao YL et al conducted a study in rural areas of China with careHPV and achieved a high sensitivity of 90% for identifying moderate or severe cervical disease (\geq CIN 2) [35]. However, low specificity was recorded, limiting the efficacy of see-and-treat programs. There is a significant need for alternative solutions to support cervical cancer screening in settings where resources are limited.

Visual inspection with acetic acid (VIA) has been explored in different developing countries as an alternative to the current paradigm [7, 31, 36, and 37]. VIA is a simple visual test, where the cervix is examined with the naked eye before and after application of acetic acid. Abnormal epithelium turns white (acetowhitening) after the application of acetic acid. VIA was evaluated in different studies, with more than 65,000 women from nine (9) different countries. The sensitivity of VIA varied from 67% to 79% and specificity ranged from 49% to 86% [38-43]. VIA is inexpensive, requires minimal infrastructure and allows for immediate treatment, eliminating the need for histological analysis. However, VIA is subjective, hence extensive training of the health-care provider is required, also consistent criteria for a suspicious lesion need to be precisely defined. In the hands of an expert, VIA can be effectively implemented, Jeronimo et al. substantially improved the diagnosis in a study involving almost 2000 women in Peru, with positivity rate dropping from 13.5% to 4% [31]. This was believed to have resulted from the experience acquired during these first few months in the study. Many other strategies including visual inspection with acetic acid and magnification (VIAM), visual inspection with Lugol's iodide (VILI) have been explored in developing countries with promising results but all these are subjective. For proper evaluation there is a great need for experienced personnel that are limited in these areas.

2.4 Optical Imaging Systems

Recent developments in optics have led to new, portable imaging systems with the potential to image cells or tissue to reveal architectural and morphologic disease characteristics without need for tissue removal. Optical imaging has the capability to obtain and display both wide-field and high-resolution images of epithelial tissues in real-time [44]. Different optical technologies that detect relative changes in the way light interacts with tissue have been developed to aid in early cancer detection; these include reflectance imaging and spectroscopy, fluorescence imaging and spectroscopy, and Raman spectroscopy. Supplementing conventional imaging with the use of polarized light, narrowband reflectance, and/or fluorescence imaging modes has been shown to improve sensitivity and specificity for several types of cancer, by reducing specular glare, enhancing vascular contrast, and detecting alterations in tissue fluorescence associated with the presence of disease. Digital optical imaging systems for cervical precancer have been developed using these principles [45-49].

2.4.1 Role of optics in cancer

Light scattering and absorption: Reflectance of light occurs when photons incident on tissue are back-scattered without a change in wavelength. Scattering in tissue arises due to differences in the refractive index between extracellular, cellular, and sub-cellular components. Angular measurements of elastic scattering from cells show nuclei and other cytoplasmic organelles cause scattering [50]. Normal epithelium scatters light differently from precancerous or cancerous epithelium; this is due to the increased nuclear size and optical density of the nucleus in an abnormal epithelium [51- 53]. Arifler, et al. found that scattering decreases in the stroma of dysplasia and is also dependent on depth in the epithelium, with scattering decreasing

in the intermediate layer compared to the superficial and basal layers [52]. Contrast agents like acetic acid have been found to increase light scattering from cervical cell nuclei [54]. Some studies have showed the mean scattering coefficient of precancerous tissue is as high as three times as that of normal epithelium [55, 56].

Not all light is scattered, some is absorbed by chromophores present in the tissue. Hemoglobin is one of the major absorbers found in stromal vasculature, and plays a major role in light absorption. As the tissue becomes more dysplastic, microvessel density also increases greatly, and hemoglobin absorption may be increased [57].

Fluorescence: Exciting tissue with ultraviolet (UV) or visible light can result in emission of

fluorescent
light at a
longer
wavelength.
Tissue
contains
fluorophores
such as
crosslinks in
collagen and

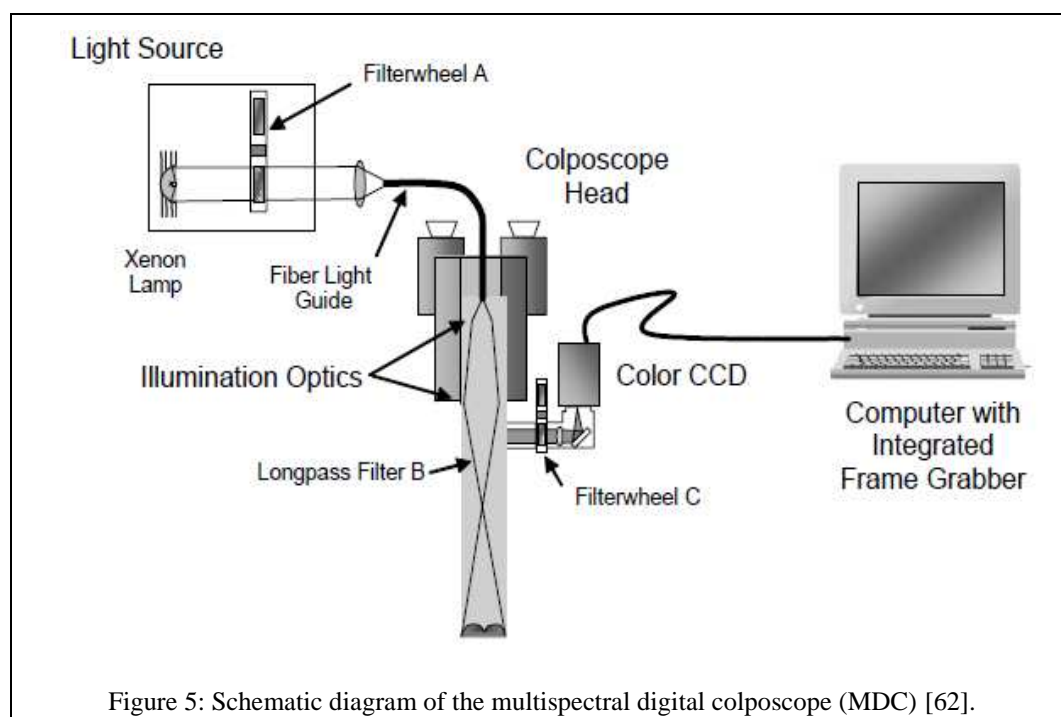


Figure 5: Schematic diagram of the multispectral digital colposcope (MDC) [62].

elastin, cellular metabolism enzymes, and aromatic amino acids [58]. Fluorescence interrogation can help detect a range of biochemical changes. In normal tissue, collagen crosslinks result in

bright fluorescence in the stroma, but this bright fluorescence is greatly decreased in cervical precancer and cancers [59-61].

2.4.2 Wide-field Imaging Systems

Wide-field imaging systems [62, 63] enable a relatively large field of view (50-100 mm) to be visualized at moderate resolution under conventional white-light illumination, as well as in fluorescence and polarized light modes. Advances in wide-field, narrow-band reflectance imaging can also be utilized to enhance vascular contrast. Wide-field imaging can screen a relatively large tissue area with high sensitivity, highlighting regions suspicious for cancer. A number of researchers have embarked on studies investigating hyperspectral autofluorescence and reflectance imaging [64-67]. Orfanoudaki et al. evaluated a wide-field, multispectral reflectance imaging system in a study involving 123 women. The system improved the diagnosis as the false positive-diagnostic rate was found to be 1.7%, compared to 22% and 24.4% of conventional colposcopy and Pap test respectively [68]. Exciting tissue fluorescence with UV and blue wavelengths 440-470nm has been extensively studied and has shown great contrast between normal and precancerous tissue [62, 69]. Ferris et al investigated a hyperspectral wide-field imaging system and found sensitivity of 97% and specificity of 70% [66]. Using the same system in a larger study of 572 women, DeSantis et al, found a sensitivity of 95.1% and a specificity of 55.2% for distinguishing between normal and high-grade precancer [67]. Similar results of a sensitivity of 92% and specificity of 50% were found in a different study involving 604 women, using a different hyperspectral imaging system [64]. The USA FDA in 2006 approved a trimodal imaging system termed; LUMATM. LumaTM uses 337nm UV nitrogen laser for fluorescence and two xenon flash lamps for reflectance. This system was evaluated in two

prospective, randomized controlled studies. A 22% gain in the true-positive rate from 193 women study [70], similar results of about 26.5% gain in true-positive with only a 4% increase in false-positive rate versus that of colposcopy alone were obtained in a multicenter study involving 2,299 women [65].

Our lab developed a Multispectral Digital Colposcope MDC [62] to measure multispectral autofluorescence and reflectance images of the cervix. The MDC (Fig. 5) is a modified standard colposcope with the ability to measure reflectance and fluorescence images. A video camera adapter was also incorporated. A color CCD camera was used to capture the images. Two excitation wavelengths 330 and 440nm showed the greatest diagnostic power relative to histology [62]. In a different study, the MDC achieved sensitivity and specificity of 79% and 88% respectively in distinguishing high-grade precancer from low-grade precancer or normal tissue [63]. Roblyer et al developed a wide-field screening system for detection of oral neoplasia. This system is a multispectral imaging system capable of acquiring white light, cross-polarized, narrow-band reflectance and fluorescence [71]. Fluorescence excited at 405 nm was established as the best mode to discriminate between normal and dysplastic/cancerous oral tissue, with the normalized ratio of red-to-green fluorescence. Sensitivity and specificity of 100% and 91.4% respectively were achieved in a 67 patient study [72]. This system led to the development of a low-cost, portable system, termed the Portable Screening System (PS2). It consists of a commercially available surgical headlight system with loupes, LEDs, excitation and emission filters, a head-mounted CCD camera, and a compact lithium-ion battery. All components are battery powered. The PS2 acquires cross-polarized white light and fluorescence images [73]. The PS2 has been used in clinical pilot studies to assess the ability to help differentiate between normal, dysplastic and cancerous oral tissue [74]. In contrast to the images from the normal

tissue, the autofluorescence signal from dysplastic tissue shows a characteristic loss of autofluorescence.

2.4.3 High-Resolution Imaging Systems

Due to the limited spatial resolution of wide-field systems, researchers embarked on ways to

image at higher spatial resolution.

High-resolution

optical imaging

techniques have

been used to

observe changes

in cells that

indicate neoplastic

transformation

[75, 76]. Such

indicators may be in the form of changes in the size and internal structure of the nucleus, the

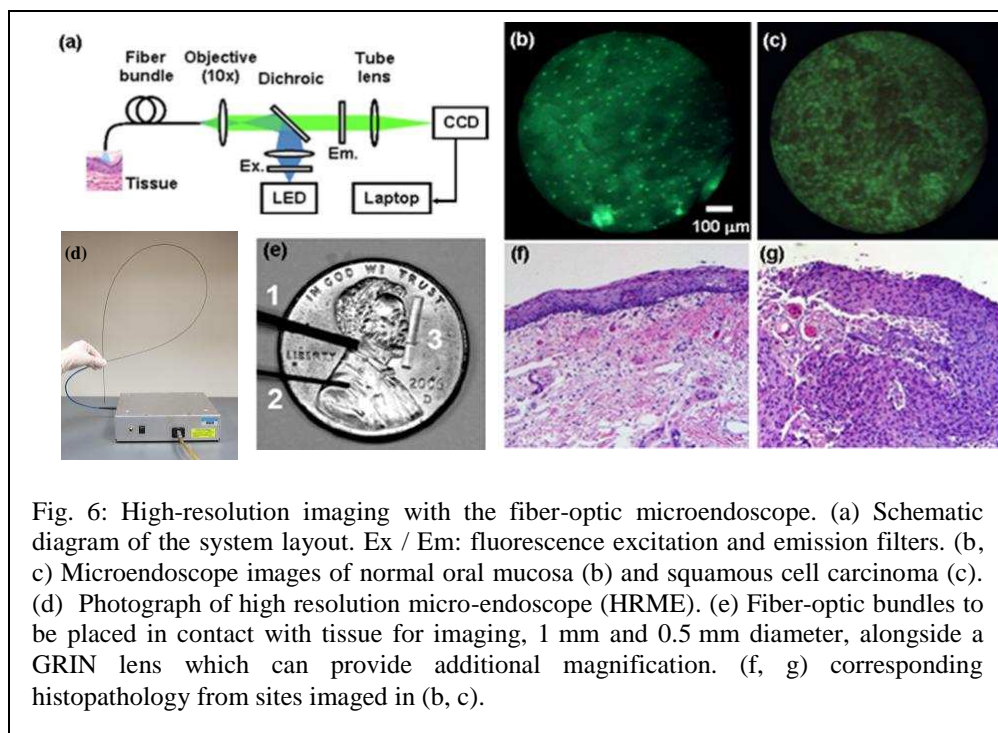
disorganization of cells, pleomorphism, and other cellular changes that require imaging with

spatial resolution on the order of a few microns. High-resolution techniques have the potential to

access indicators observed during pathological analysis such as cell morphology as well as

epithelial architecture without the need for biopsy [77] therefore lowering costs or discomfort to

the patient associated with traditional biopsy.

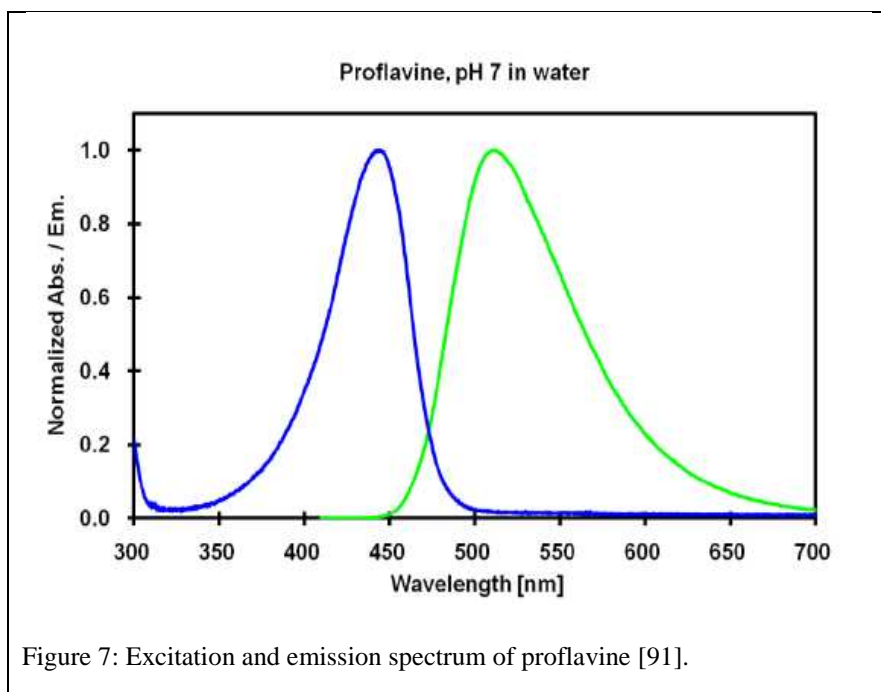


Confocal microscopy has been used for a number of years for in vitro applications, but has recently been shown to be useful for the imaging of ex vivo biopsies and in vivo tissues [55, 75, 78]. Tan et al used a confocal endomicroscopy in both reflectance and fluorescence modes, and achieved 97% sensitivity to detect CIN and 80% specificity for normal-CIN 1 and 93% specificity for CIN 2-CIN 3 [79]. Collier et al achieved sensitivity and specificity of more than 90% by measuring the nuclear cytoplasmic (N/C) ratio [75]. Despite the advantages of confocal imaging, there are significant drawbacks that limit the potential applications. First, while miniaturization of confocal systems in recent years has created progressively smaller instrumentation, including a confocal endoscope, the optical and mechanical elements of these systems have generally limited the usefulness of this technique to easily accessible regions of the body [80-87]. Second, the technical complexity and high cost of confocal imaging systems has generally limited their application to high resource settings.

Our lab has recently developed a new high resolution imaging system to address these limitations. The system consists of a fiber-optic microendoscope (Fig. 6a) termed the high-resolution microendoscope (HRME); it is based on fluorescence imaging through a flexible, 1 mm diameter fiber-optic bundle (Fig. 6e) [88]. This unit, along with a laptop computer for image display, is completely battery-powered and can be transported within a briefcase to remote settings; fig. 6d shows the photograph of high-resolution micro-endoscope (HRME). This system is being evaluated in different pilot clinical studies; include the oral cavity [88] (Fig. 6), uterine cervix and esophagus [89]. These images were acquired on ex vivo tissue specimens, following topical application of 0.05% acriflavine solution.

Representative images and histopathology of normal oral mucosa (b, f) and squamous cell carcinoma (c, g) are shown in Fig. 6, demonstrating the ability of the microendoscope to image the distribution and density

of cell nuclei within intact epithelium, following topical application of 0.05% acriflavine solution. Acriflavine is a fluorescent dye, which can be used to selectively label cell nuclei due to its ability to bind to DNA. In Fig. 6b, nuclei of normal epithelium appear



bright and sparsely distributed, while in Fig. 6c, nuclei appear crowded throughout the 800 nm diameter field-of-view; these features are seen in histology (Fig. 6f, g).

2.5 Proflavine

Proflavine is an acriflavine derivative, which has been used as a topical antiseptic. Proflavine is known to be able to label DNA in a nucleus of cells by intercalating between nucleic acid base pairs [90]. Although proflavine is not a molecular-specific agent, its binding to DNA distinguishes nuclei from the cytoplasm of the cell with nuclei appearing bright. High-resolution fluorescence imaging of this agent in tissue can give morphologic information such as the nuclear-to-cytoplasmic ratio which is an important parameter used in the histological diagnosis

of cancer [56]. Proflavine absorbs strongly at 445 nm, and it emits light with a peak around 510 nm [91] as shown in Figure 7. Topical use of proflavine has a long history of reported safe use in humans [92, 93]; it has been used extensively as a topical antiseptic [94]. I used proflavine at a relatively small dose (0.01%), as part of a one-time screening procedure to stain epithelial cells of the cervix that will naturally exfoliate in a fairly short time. Our lab has obtained IRB approval and an IND from the FDA to use to topical proflavine as a contrast agent to aid in the early detection of dysplasia in Barrett's esophagus and in the oral mucosa. We have also obtained IRB approval for topical use in the cervix.

3. HIGH-RESOLUTION MICROENDOSCOPE FOR THE DETECTION OF CERVICAL NEOPLASIA IN LOW-RESOURCE SETTINGS

The contents of this chapter have been published in the following journal article: Quinn MK, Bubi TC, Pierce MC, Kayembe MK, Ramogola-Masire D, et al. (2012) High-Resolution Microendoscopy for the Detection of Cervical Neoplasia in Low-Resource Settings. PLoS ONE 7(9): e44924. doi:10.1371/journal.pone.0044924

Abstract: Cervical cancer is the second leading cause of cancer death among women in developing countries. Developing countries often lack infrastructure, cytotechnologists, and pathologists necessary to implement current screening tools. Due to their low cost and ease of interpretation at the point-of-care, optical imaging technologies may serve as an appropriate solution for cervical cancer screening in low resource settings. We have developed a high-resolution optical imaging system, the High Resolution Microendoscope (HRME), which can be used to interrogate clinically suspicious areas with subcellular spatial resolution, revealing changes in nuclear to cytoplasmic area ratio. In this pilot study carried out at the women's clinic of Princess Marina Hospital in Botswana, 52 unique sites were imaged in 26 patients, and the results were compared to histopathology as a reference standard. Quantitative high-resolution imaging achieved a sensitivity and specificity of 86% and 87%, respectively, in differentiating neoplastic (SCIN 2) tissue from non-neoplastic tissue. These results suggest the potential promise of HRME to assist in the detection of cervical neoplasia in low-resource settings.

3.1 Introduction

Cervical cancer is the third most common type of cancer among women worldwide. In 2008, there were an estimated 530,000 new cases and more than 275,000 deaths due to cervical cancer. Over 85% of new cases of cervical cancer and deaths due to cervical cancer occur in developing countries where screening programs for early detection are either inadequate or unavailable [1].

In the United States and many other high-resource countries, organized screening programs based on the Pap (Papanicolaou) smear and human papillomavirus (HPV) tests enable early diagnosis and treatment of precancerous lesions. An abnormal Pap smear test or HPV test is followed by colposcopy. If abnormalities are evident under colposcopy, a biopsy is required to confirm disease before treatment. The widespread use of Pap smears, colposcopy, biopsy, and treatment of pre-cancerous lesions has led to dramatic reductions in the incidence and mortality of cervical cancer in the United States [95]. However, this process requires multiple patient visits and highly trained personnel to read cytology and biopsy results. In resource-constrained settings, the increased risk of patient loss to follow-up and lack of trained personnel and laboratories often make this screening paradigm ineffective. HPV testing has been explored in developing countries and the available data have demonstrated the potential of HPV testing to reduce both the mortality and long term risk of cervical cancer [96]. However, currently available HPV tests require six hours to produce a result, necessitating multiple visits for screening and treatment. More recently, rapid HPV tests have emerged which may offer a potential solution, but are yet to become commercially available [35]. Alternative early cervical cancer detection methods that are accurate, low cost, and that allow immediate diagnosis and treatment in a single visit are crucial for low-resource countries [7]. Visual inspection with acetic acid (VIA) is the most widely available screening modality in developing countries. This is a

simple visual test, in which the cervix is examined with the naked eye before and after application of 3 to 5% acetic acid (vinegar). Upon application of the acetic acid, suspicious areas turn white. VIA has been explored in various developing countries as an alternative to cytology, and has shown promising results in detecting high-grade dysplasia or invasive carcinomas [43,97]. Although not as extensively used as VIA, visual inspection with Lugol's iodine (VILI) has shown promising results compared to both Pap smear and VIA. In a multicenter study in several developing countries involving 56,939 women, the sensitivity of VIA varied from 67-79% and specificity ranged from 49%-86%, while the sensitivity and specificity of VILI varied from 76%–97% and 73%–92%, respectively [43]. VIA and VILI are inexpensive, require minimal infrastructure, allow for immediate treatment, and eliminate the need for a laboratory. Despite the advantages of

VIA and VILI over cytology, these tests are subjective, requiring extensive and ongoing training of health-care providers, and are frequently associated with low specificity, which can result in significant overtreatment.

As an alternative to visual examination of the cervix, high-resolution fiber optic microscopes are now available which facilitate direct visualization of neoplastic indicators such as elevated nuclear to cytoplasmic area ratio, nuclear crowding, and pleomorphic nuclei. These indicators are conventionally only observed during cytologic or histologic analysis following an invasive biopsy. Vital dyes can provide high optical contrast if applied topically. For example, proflavine, a fluorescent DNA label, distinguishes nuclei from the cytoplasm of the cell with nuclei appearing bright. Proflavine has peak absorbance at 445 nm and a peak emission at 510 nm. High-resolution fluorescence imaging of this agent in tissue can yield morphologic information such as the nuclear-to-cytoplasmic ratio which is an important parameter used in the histological

diagnosis of cancer. It has a long history of safe clinical use as a topical antiseptic [93,92], and is a component of acriflavine, which has been used in clinical imaging studies of the gastrointestinal tract and cervix [98,79].

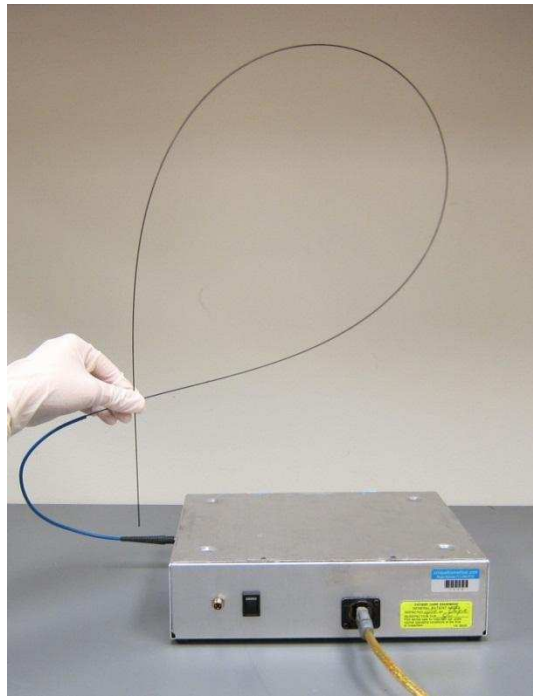


Figure 8: Photograph of high-resolution micro-endoscope (HRME)

Due to their low cost and ease of interpretation at the point-of-care, high resolution optical imaging technologies may serve as an appropriate solution for cervical cancer screening in low resource settings [76]. We recently developed a high-resolution microendoscope (HRME) to address the limitations of conventional methods of cervical cancer screening. The HRME has been evaluated in pilot studies of oral and esophageal precancer diagnosis [99–101]. In these studies, proflavine is applied topically to the squamous epithelium, and the area is interrogated with a fiber-optic bundle. Changes in cell morphology and epithelial architecture can be visualized in real time on a laptop computer. The objective of this study was to evaluate the

ability of this high-resolution microendoscope to identify cervical neoplasia in patients at the women's clinic at Princess Marina Hospital in Botswana. Images were acquired from 52 sites in 26 patients. The images acquired by the microendoscope were assessed by both visual inspection by two expert observers and quantitative analysis to discriminate neoplastic (\geq CIN 2) from non-neoplastic cervical tissue. Results were compared to histopathology as the reference standard.

Diagnostic Category	Histopathology Diagnosis	Number of Sites Imaged
Normal/Benign	Normal	5
	Inflammation	7
LGSIL	HPV Effect	11
	CIN I	7
HGSIL	CIN 2	2
	CIN 3	12
Total Number of Sites Imaged		44

Table 1. Number of sites imaged by HRME, grouped according to histopathology diagnosis.

3.2 Materials and Methods

3.2.1 Instrumentation

Images were acquired using a custom designed, low cost high-resolution microendoscope (HRME); this system has been described in detail previously [102]. Briefly, the HRME is a fiber optic fluorescence microscope, which can acquire images of tissue with sub-cellular resolution at video-rate. As shown in Fig. 8, the HRME consists of a coherent, flexible 1 mm diameter fiber

bundle (Sumitomo, IGN-08/30) coupled to a light source and a digital CCD camera. Light from a blue LED with peak wavelength centered at 455 nm (Thorlabs, FB450-40) provides illumination; fluorescence emission from the tissue is collected by the bundle, transmitted through a 475 nm dichroic mirror (Chroma, 475DCXRU), and focused onto an optical sensor of the CCD camera (Point Grey Research, GRAS-14S5C-M) by an objective lens (106/0.25) and a 150 mm tube lens. Images are transferred to a laptop via IEEE-1394 (Firewire) cable. The field of view of the HRME is 720 mm in diameter, and the lateral spatial resolution is approximately 4 mm.

3.2.2 Clinical Measurements

Women attending a colposcopy clinic on the basis of an abnormal Pap smear were eligible to participate in the study if they were at least 18 years of age and not pregnant. A health care provider described the procedure to eligible patients; patients who agreed to participate were provided with and signed forms indicating informed consent and authorization. Study participation included colposcopic examination of the vulva, vagina, and cervix using 3% acetic acid. Abnormal cervical lesions in the transformation zone were identified and noted by the study physician, in accordance with routine patient care. Each lesion was described and classified by the study physician as clinically high grade, clinically low grade, or clinically normal using the Reid Colposcopic Index [103]. Following routine colposcopic examination, a solution of proflavine hemisulfate (0.01% w/v in sterile phosphate buffered saline) was topically applied to the cervix with a cotton swab. Following application of proflavine, the HRME was advanced through the speculum and placed in gentle contact with the cervix. Three second movies were obtained by the HRME from up to two clinically abnormal cervical sites and one clinically normal cervical site in the transformation zone. Following optical measurements, all

sites interrogated with the HRME probe were biopsied and submitted for routine histopathologic analysis. A single pathologist who was blinded to the results of the optical imaging read biopsies. Diagnostic classification categories included normal, inflammation, HPV effect, grade 1 cervical intraepithelial neoplasia (CIN 1), grade 2 cervical intraepithelial neoplasia (CIN 2), and grade 3 cervical intraepithelial neoplasia (CIN 3) using standard histopathologic criteria [104]. Squamous metaplasia was considered a normal result. No cases of carcinoma in situ (CIS) or squamous cell carcinoma (SCC) were observed in this study. Low-grade dysplasia includes HPV effect and CIN 1, and high grade dysplasia includes CIN 2 and CIN 3. Normal/benign results included inflammation. For purposes of data analysis, neoplastic tissue was classified as high grade dysplasia, and all other diagnoses were considered to be non-neoplastic.

3.2.3 Data Analysis

For each HRME movie, one representative frame was chosen which minimized motion artifact and obstruction of the field of view due to cellular debris. The user selecting the frames was blinded to all diagnostic information. The resultant HRME images were reviewed for quality control by a reviewer blinded to all diagnostic information. Images were discarded if more than 50% of the field of view was out of focus, contained evidence of motion artifact, or contained significant debris. HRME images that passed quality control and had a corresponding histopathologic diagnosis were analyzed in two ways.

First, images were reviewed by two expert observers, who had each previously reviewed HRME images from more than 50 cases of normal and neoplastic tissues. HRME images passing quality control were presented to each reviewer in randomized order; reviewers were instructed to classify each image as non-neoplastic or neoplastic. The sensitivity and specificity of

qualitative analysis was calculated for each reviewer using histopathologic diagnosis as the reference standard.

Second, image analysis software was used to analyze each HRME image which passed quality control to calculate quantitative image features. Analysis focused on assessment of nuclear size, since changes in nuclear size and nuclear-to-cytoplasmic ratio are hallmark histopathologic features of cervical precancer [105]. A reviewer, blinded to the histopathologic diagnosis, first manually selected a region of interest (ROI) for quantitative analysis. The ROI was selected to include regions with visible nuclei and to exclude regions with evidence of motion artifact, image saturation, or debris. Following selection of the ROI from an HRME image, image contrast was adjusted using a contrast-limited adaptive histogram equalization, and median filtering was applied to remove the background pattern associated with the structure of the fiber bundle. Each processed gray-scale image was then converted to a binary image using a threshold value. A reviewer, again blinded to the histopathologic diagnosis, reviewed the binary images and adjusted the threshold value to ensure that nuclei were segmented appropriately based on visual assessment. Binary images were then processed to remove all objects with fewer than 50 pixels (assumed to be noise) and more than 1500 pixels (assumed to be debris). Finally, for each image the mean nuclear to cytoplasmic area (N/C) ratio was calculated by dividing the total nuclear area by the total cytoplasmic area within the ROI.

3.2.4 Ethics Statement

The study protocol was reviewed and approved by the Institutional Review Board at Rice University and the Health Research Division Office of the Botswana Ministry of Health.

Written informed consent documents were available in both English and the local national language (Setswana). All patients involved in the study gave written informed consent.

Results

HRME images were acquired from 52 sites in 26 patients. Images from 8 sites were excluded from further analysis because they did not pass quality control criteria outlined above. The rejection of the 8 sites eliminated all data from one subject. For this subject, the two movies collected were both out of focus because the distal tip of the probe was not in contact with the cervical epithelium. Table 1 summarizes the histopathologic diagnoses of the remaining 44 sites. The majority of patients in the study were human immunodeficiency virus (HIV) infected, which has been correlated with a high incidence of intraepithelial lesions [106].

Figure 9 shows typical HRME images of clinically and histopathologically normal (a–c) and neoplastic (d–f) cervical tissues. The top row shows a colposcopic photograph of the cervix; the white arrow indicates the clinically normal site where the HRME probe was placed. The corresponding HRME image shows small, regularly spaced nuclei. Both expert reviewers considered this image qualitatively non-neoplastic, which was consistent with the histopathologic diagnosis of HPV effect. The bottom row shows a colposcopic photograph indicating a clinically abnormal thick aceto-white lesion (white arrow). The HRME image obtained from this site shows large, crowded, pleomorphic nuclei. The image was considered qualitatively neoplastic by both expert observers, which was consistent with the histopathologic diagnosis of CIN 3.

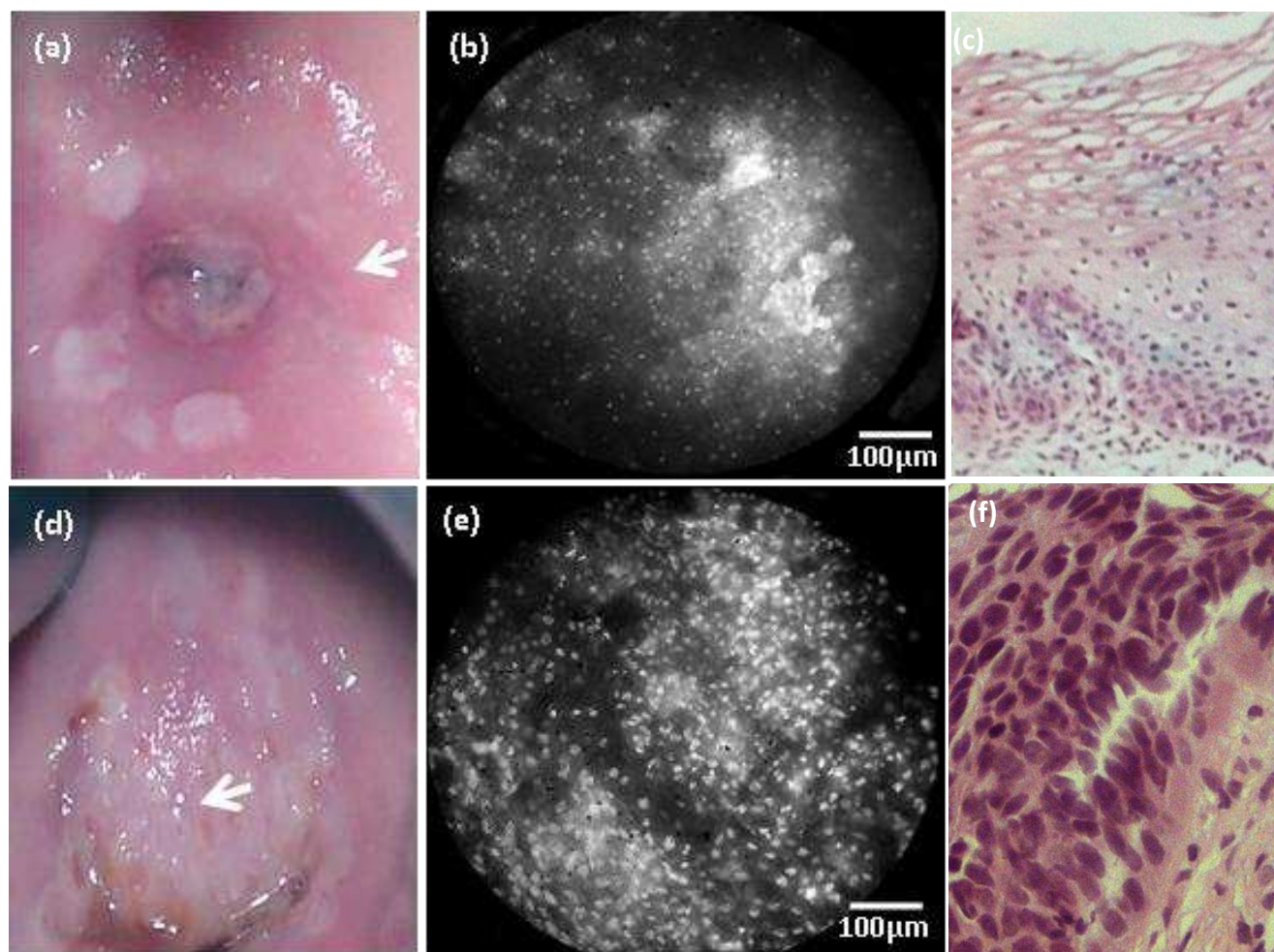


Figure 9. Comparison of colposcopic appearance, HRME images, and histologic diagnosis. The top row shows images obtained from a clinically normal region of the cervix. The white arrow in the colposcopic image (a) indicates the area imaged with the HRME. The HRME image (b) shows small, uniformly spaced nuclei, and was considered non-neoplastic by both subjective expert observers, which is consistent with histopathology indicating HPV effect (c). The bottom row shows images from a clinically abnormal region of the cervix. The white arrow in the colposcopic image (d) indicates a region with a clinical impression of high grade disease. The corresponding HRME image (e) shows large, pleomorphic, crowded nuclei and was considered neoplastic by both subjective expert observers, which is consistent with histopathology indicating CIN3 (f).

Figure 10 shows HRME images obtained from a case in which the colposcopic impression did not agree with the histopathologic diagnosis. The colposcopic photograph shows a warty lesion (white arrow) which was classified as clinically high grade disease according to the Reid Colposcopic Index. The HRME image obtained from this site showed small nuclei, characteristic of normal epithelium. The expert reviewers categorized this image as non-neoplastic. This was consistent with the histopathologic diagnosis of HPV effect.

Qualitative diagnoses by the expert HRME observers for all 44 sites were compared with histopathologic diagnosis to calculate sensitivity and specificity. Observer #1 classified the images with a sensitivity and specificity of 86% and 70% respectively. Observer #2 classified the images with a sensitivity and specificity of 93% and 73% respectively.

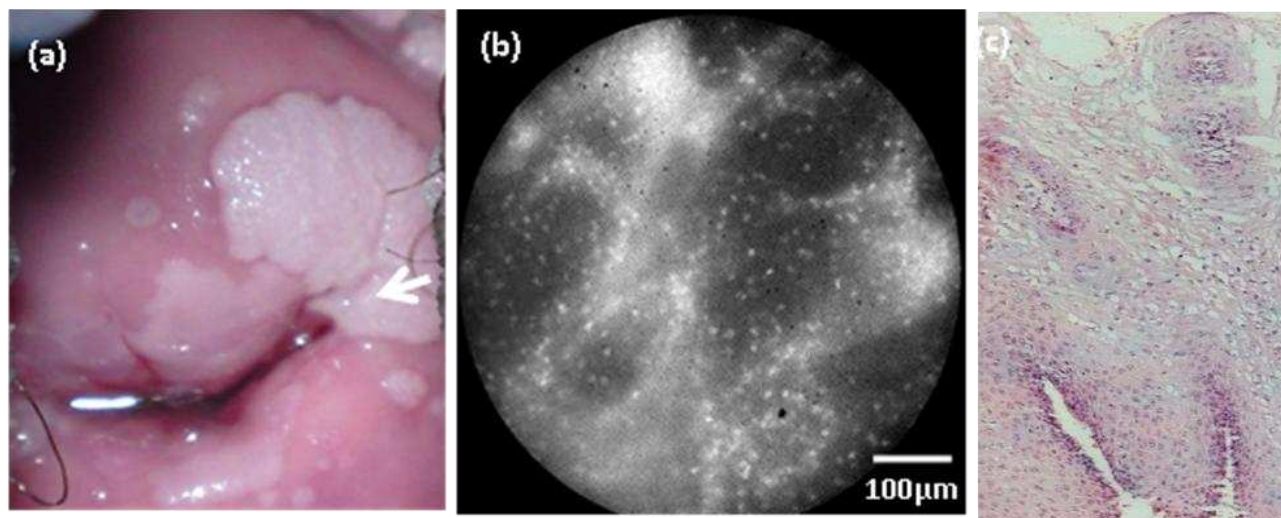


Figure 10. Comparison of colposcopic appearance, HRME images, and histologic diagnosis in a case where colposcopic impression did not agree with histopathologic diagnosis. The white arrow in the colposcopic image (a) indicates the area imaged with the HRME; the clinical impression of this warty looking lesion was high grade disease according to the Reid Colposcopic Index. The HRME image (b) shows small, uniformly spaced nuclei. This image was considered qualitatively non-neoplastic by both subjective expert observers, which is consistent with the histologic image indicating HPV effect (c).

Quantitative morphometric image analysis was next performed;

Figure 4 illustrates results from representative HRME images of non-neoplastic and neoplastic tissues. In each image, the user defined ROI is outlined in green; within this ROI, the automatically segmented nuclei are outlined in red. ROI size did not vary significantly from neoplastic images to non-neoplastic images (Student's t-test, $p < 0.5$). Figure 11a shows an HRME image from a site histopathologically diagnosed as HPV effect; the N/C ratio was 0.08. In

contrast, Fig. 11b shows an HRME image from a site diagnosed as CIN 3 with an N/C ratio of 0.22.

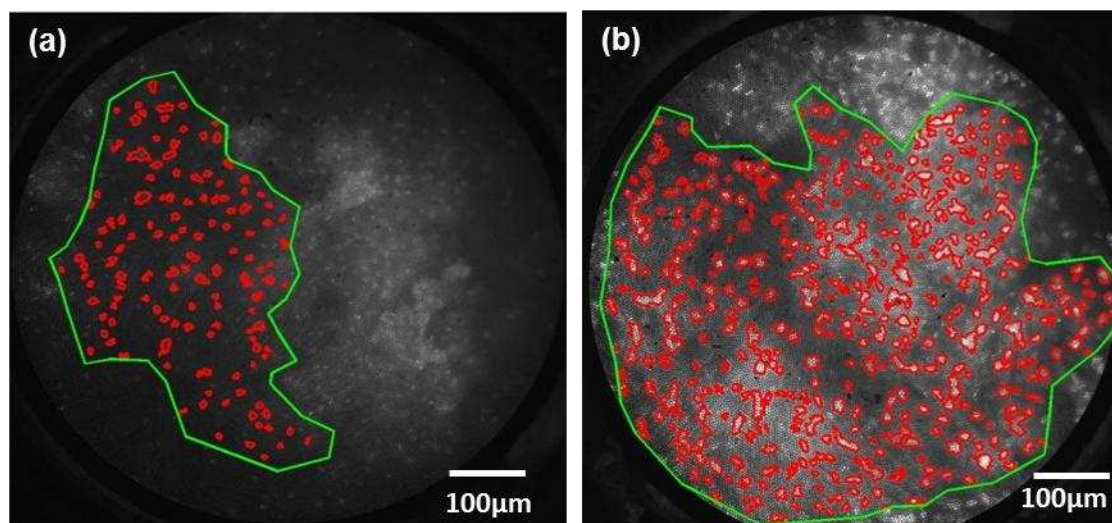


Figure 11. HRME images were analyzed to calculate the average nuclear to cytoplasmic (N/C) area ratio. A region of interest (green) was defined by the user to select regions of the image with visually observable nuclei. Within this region, a computer program segmented nuclei and calculated the N/C area ratio. Representative images showing a site diagnosed as HPV with an N/C ratio of 0.08 (a) and site diagnosed as CIN 3 with an N/C ratio of 0.22 (b) are shown.

To assess whether differences in the N/C ratio as measured from HRME images correlated with histopathologic diagnosis, we grouped sites by histopathologic diagnosis and calculated the mean of the N/C ratio (Fig. 12). Results show that the average N/C ratio increases with increasing grade of neoplasia; the mean N/C ratio of sites diagnosed as high grade dysplasia was significantly higher than those diagnosed as normal/benign (Student's t-test, $p = 2.061025$) and those diagnosed as low grade (Student's t-test, $p = 1.961025$).

Figure 13 shows a scatter plot indicating the N/C ratio vs. histopathologic diagnosis for each of the 44 sites measured in this study. We explored whether this parameter could be used to classify sites as neoplastic (high grade dysplasia) or non-neoplastic (normal/benign or low grade dysplasia). Using a simple cut-off where sites with an N/C ratio greater than 0.163 were diagnosed as neoplastic and sites with an N/C ratio of less than 0.163 were classified as non

neoplastic correctly classified 12 of 14 sites with a histopathologic diagnosis of high grade, 16 of 18 sites with a histopathologic diagnosis of low grade, and 10 of 12 sites with a histopathologic diagnosis of normal/benign.

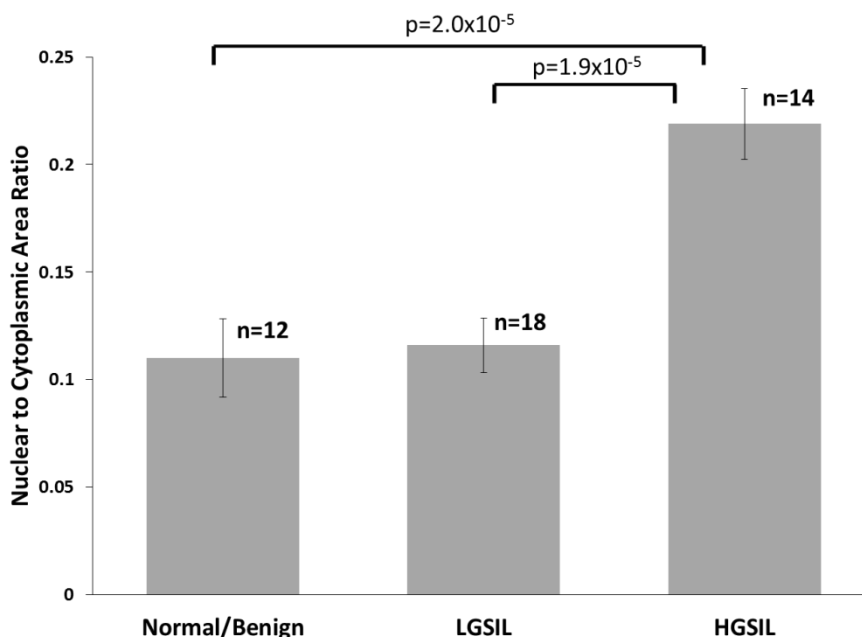


Figure 12. The average N/C ratio versus histopathologic diagnosis by diagnostic category. The average N/C ratio of sites diagnosed as high grade dysplasia was significantly higher than those diagnosed as normal/benign (Student's t-test, $p = 2.0E-5$) and low grade dysplasia (Student's t-test, $p = 1.9E-5$). Error bars indicate standard error.

The receiver operator characteristic (ROC) curve for a diagnostic algorithm based on the N/C ratio is shown in Fig. 14. The Q-point indicated on the figure corresponds to the cut-off value shown in Fig. 13, and corresponds to a sensitivity of 86% and a specificity of 87%. Figure 14 also shows the accuracy of visual interpretation of the HRME images by two observers relative to the reference standard of histopathology. For both observers, the accuracy of visual image interpretation lies near the ROC curve for quantitative image interpretation. For comparison, the sensitivity and specificity of clinical colposcopic impression for the same sites were 64% and 83%, respectively when clinically low-grade lesions were considered non-neoplastic.

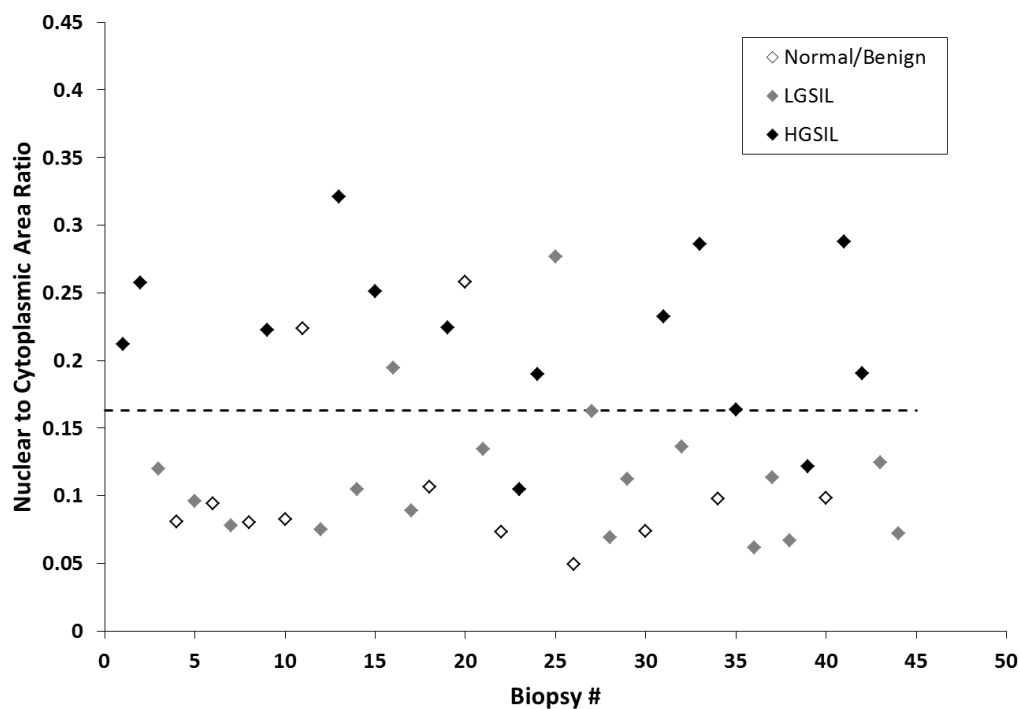


Figure 13. Scatter plot of N/C ratio for all samples, broken down by histopathologic diagnosis. The dotted line indicates a threshold at 0.163 with a sensitivity of 86% and a specificity of 87% for separating samples diagnosed as high grade dysplasia from samples diagnosed as low grade dysplasia or normal/benign.

Discussion

This study suggests that high-resolution microendoscopy shows promise to improve cervical cancer screening in resource-constrained settings. In this pilot study, both the sensitivity and specificity of HRME based detection were higher than that of colposcopic impression. While encouraging, our study has a number of limitations. First, it was a pilot study involving only 52 sites in 26 patients. A larger, prospective study is required to confirm the results. Second, all HRME images were acquired from colposcopically suspicious and normal areas in the transformation zone. We have not characterized HRME images of endocervical tissue to

determine whether they may be a potential source of error. Although all data in this study was taken from the transformation zone of the cervix as identified by the physician, three biopsies were noted to contain predominantly columnar epithelium by pathology. Further research is necessary to identify the differences between HRME images of dysplastic squamous epithelium, normal columnar epithelium, and dysplastic columnar epithelium.

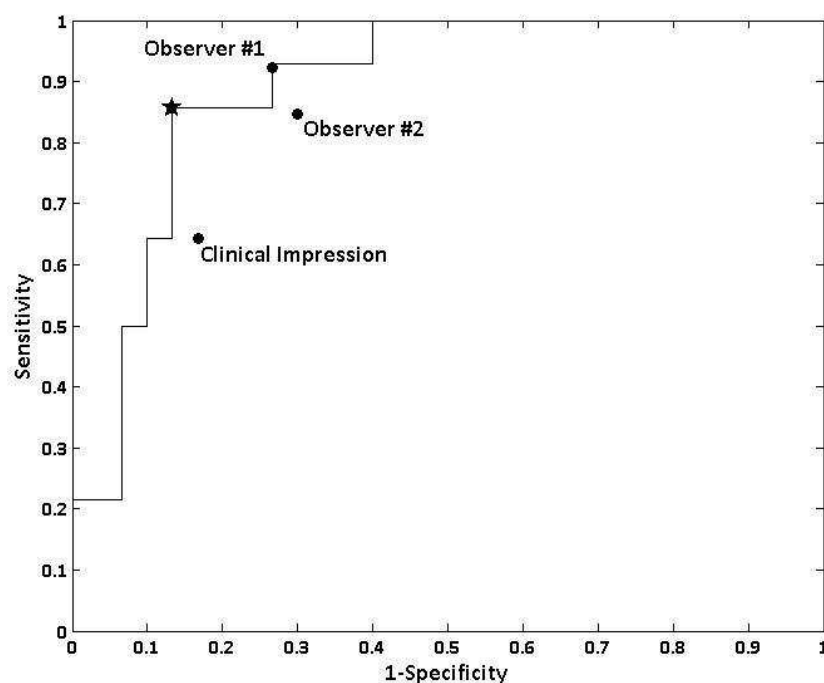


Figure 14. Receiver operator characteristic curve for the algorithm shown in Figure 6. The star indicates the Q-point, with a sensitivity of 86% and a specificity of 87%. The performance of visual interpretation of HRME images by two observers is indicated and falls along the ROC curve for automated image analysis. For comparison, the sensitivity and specificity of clinical colposcopic impression for the same sites were 64% and 83%, respectively.

High-resolution imaging offers a number of potential advantages as a screening tool. Studies of VIA have shown a wide range of resulting sensitivities and specificities. A metastudy of VIA, which included Sankaranarayanan's multicenter study, revealed sensitivities ranging from 41%–92% and specificities ranging from 49%–98% [107]. This significant variation in

accuracy calls for additional measures to maintain consistency of diagnoses. The HRME system could potentially act as additional test to VIA and VILI screening systems.

When VIA and VILI screening systems refer patients for additional treatment, providers in low resource settings can choose to screen and provide care in one visit. The “see and treat” system eliminates biopsies to confirm disease in visible lesions before a loop electrosurgical excision procedure (LEEP) or cautery [108]. Our results suggest that the HRME shows promise as a reliable alternative to a biopsy at this second line of care in resource-constrained areas. In particular, the high specificity of the HRME results indicates that high-resolution microendoscopy could potentially lower the number of overtreated lesions.

4. HRME VALIDATION PAPER

4.1 INTRODUCTION

Despite being almost 100% curable when detected early [6], cervical cancer continues to be a major health problem for women in developing countries. In 2008, there were an estimated 235,000 deaths in developing countries due to cervical cancer compared to just over 41,000 deaths in developed countries [1]. In 2002, cervical cancer incidence and mortality rates were nearly 6 and 15 times higher in sub Saharan Africa than in North America [2]. Parkin et al estimate that by the year 2020, 90% of the mortality of cervical cancer will occur in developing countries if no major interventions are carried out [2].

Disparities in the incidence and mortality of cervical cancer between developed and developing countries arise mainly due to the uneven distribution of healthcare resources. In developed countries where organized screening and early detection programs have been implemented, the incidence and mortality rates are greatly reduced. This reduction is largely credited to the use of Papanicolaou (Pap) smear screening, followed by colposcopic diagnosis, and treatment of neoplastic lesions [109]. However, this process requires multiple patient visits to the clinic and highly trained personnel to read cytology and pathology, making it difficult to implement in resource-limited settings.

A number of cost-effective screening techniques have been investigated for use in low-resource countries, including visual inspection using either acetic acid (VIA) or Lugol's iodine (VILI) [-7, 36,43, 110]. Although encouraging results have been reported, these tests have low specificities, resulting in high rates of overtreatment, which wastes scarce resources.

Since cervical neoplasia is caused by persistent infection of the cervix with human papillomavirus (HPV), HPV DNA testing has been explored as an alternative screening

approach. In most cases, HPV testing demonstrated similar or better sensitivities compared to VIA and Pap smear screening [7, 96, 110]; however, currently available HPV tests require a fully functioning laboratory and test results are not immediately available, making widespread implementation difficult in developing countries.

High-resolution optical imaging has also been investigated as alternative approach to improve early detection. Optical images of cervical epithelium can be obtained in real time without the need for biopsy; resolution is sufficient to visualize changes in cell morphology and epithelial architecture that are characteristic of cervical neoplasia. Both confocal reflectance and fluorescence microscopy have shown promising results to aid in early detection of cervical neoplasia in *ex vivo* and *in vivo* studies [45, 56, 75, 79]. Tan et al [79] used *in vivo* confocal endomicroscopy in reflectance (following application of 6% acetic acid) and fluorescence (following application of acriflavine) modes, demonstrating the ability of confocal microscopy to visualize nuclear morphology in the cervical epithelium; the resulting images could be used to identify cervical neoplasia with a sensitivity and specificity of 97% and 93%, respectively. While promising, the technical complexity and high cost of confocal imaging systems have limited their use to high resource settings.

Recently, we developed a new high resolution optical imaging system with promise for *in vivo* detection of cervical neoplasia in low resource settings; the high-resolution microendoscope (HRME) is a battery powered, fiber optic fluorescence which can obtain images of epithelial tissue at 15 frames per second with a spatial resolution of 4 μm and a field of view of 750 μm . The affordable system can be transported in a briefcase for use in remote settings.

Several pilot studies have been carried out using the HRME to explore the ability to discriminate neoplastic and non-neoplastic tissues in the oral cavity [99] and breast [112]. The

HRME was used to acquire in vivo images of cervical epithelium in Princess Marina Hospital in Botswana, a low-resource setting with a high prevalence of cervical cancer [111]. In that study, 44 sites were imaged and an image analysis algorithm was developed to distinguish neoplastic and non-neoplastic tissue. Using only the mean nuclear to cytoplasmic area ratio, the algorithm achieved a sensitivity of 86% and specificity of 87% compared to the reference standard of histology. To more objectively evaluate the potential utility of this approach requires that the algorithm performance be evaluated with an independent data set. The goal of this study was to test the reliability and reproducibility of these results using the same algorithm in the same low-resource setting. A total of 128 sites from 60 subjects were imaged; HRME images from each measured site were analyzed quantitatively using the same image analysis procedure to discriminate neoplastic (HGSIL or cancer) from non-neoplastic tissue (normal/benign or LGSIL). Results were compared to the gold standard of histopathology.

4.2 MATERIALS AND METHODS

4.2.1 Study Population

This study was conducted at Princess Marina Hospital (PMH), Gaborone, Botswana. The study was reviewed and approved by the Institutional Review Boards at PMH and at Rice University. Patients referred for colposcopy because of an abnormal Pap smear, aged ≥ 18 years and not pregnant were eligible to participate in the study. The procedure was fully described by the research nurse and a signed informed consent obtained from all study participants.

Patients underwent standard-of-care colposcopic examination, during which the study physician identified, described and classified the abnormal cervical lesions using standard clinical criteria [103]. Following colposcopy, a solution of proflavine hemisulfate (Sigma-

Aldrich, P2508) dissolved in sterile phosphate buffered saline at a concentration of 0.01% (w/v) was topically applied to the cervix with a cotton swab. Immediately after application of proflavine, the HRME probe was placed in gentle contact with a site in the transformation zone and three second movies were recorded. Several sites in each patient were selected by the clinician for HRME measurement, including up to two clinically suspicious lesions and one site with a normal clinical appearance. Upon completion of the optical measurements, biopsy specimens were collected from the measured sites and then submitted for routine histopathologic evaluation. The study pathologist's diagnoses were categorized as normal, inflammation, squamous metaplasia, HPV infection, grade 1 cervical intraepithelial neoplasia (CIN 1), grade 2 cervical intraepithelial neoplasia (CIN 2), and grade 3 cervical intraepithelial neoplasia (CIN 3). Low grade dysplasia included HPV effect and CIN1 and high grade dysplasia included CIN2 and CIN3. Normal, inflammation squamous metaplasia, and low-grade dysplasia were defined as non-neoplastic. High-grade dysplasia was defined as neoplastic tissue.

	Diagnostic Category	Histopathology Diagnosis	Number of Sites Imaged
Non-neoplastic	Normal/Benign	Normal	9
		Inflammation	7
	Low Grade Dysplasia	HPV Effect	33
		CIN 1	8
Neoplastic	High Grade Dysplasia	CIN 2	8
		CIN 3	34
	Total		99

Table 2: Number of sites imaged by HRME, grouped according to histopathology diagnosis.

4.2.2 Data analysis

Images were visually evaluated for quality control by two observers who were blinded to the histologic diagnosis. Images were discarded if more than 50% of the field of view appeared to be out of focus and contained significant debris, if there was evidence of motion artifact, or if it appeared that the fiber-optic probe was not in contact with the tissue..

Image analysis software was written (Matlab R2010b) to quantify image features associated with cervical precancer. This software has been described in detail previously [111]. Briefly, a region of interest (ROI) was selected from each image by an observer who was blinded

to both clinical impression and histologic diagnosis; the ROI was chosen from areas of the image illustrating cellular detail, avoiding regions with evidence of motion artifact, out of focus, or debris. The ROI from each image was then analyzed as follows. First, image contrast was adjusted and the ROI was median filtered to eliminate the structure of the fiber bundle. The resulting image was then converted to a binary image and a threshold applied to segment nuclei. Morphologic processing was applied to remove noise from the image; segmented regions that contained fewer than 50 pixels were removed as they were assumed to be “noise” while objects that contained more than 1500 pixels were removed because they were thought to be debris. Finally, the number of pixels corresponding to nuclei were summed and divided by the total number of pixels in the ROI (minus nuclei), to yield the nuclear-to-cytoplasmic area (N/C) ratio.

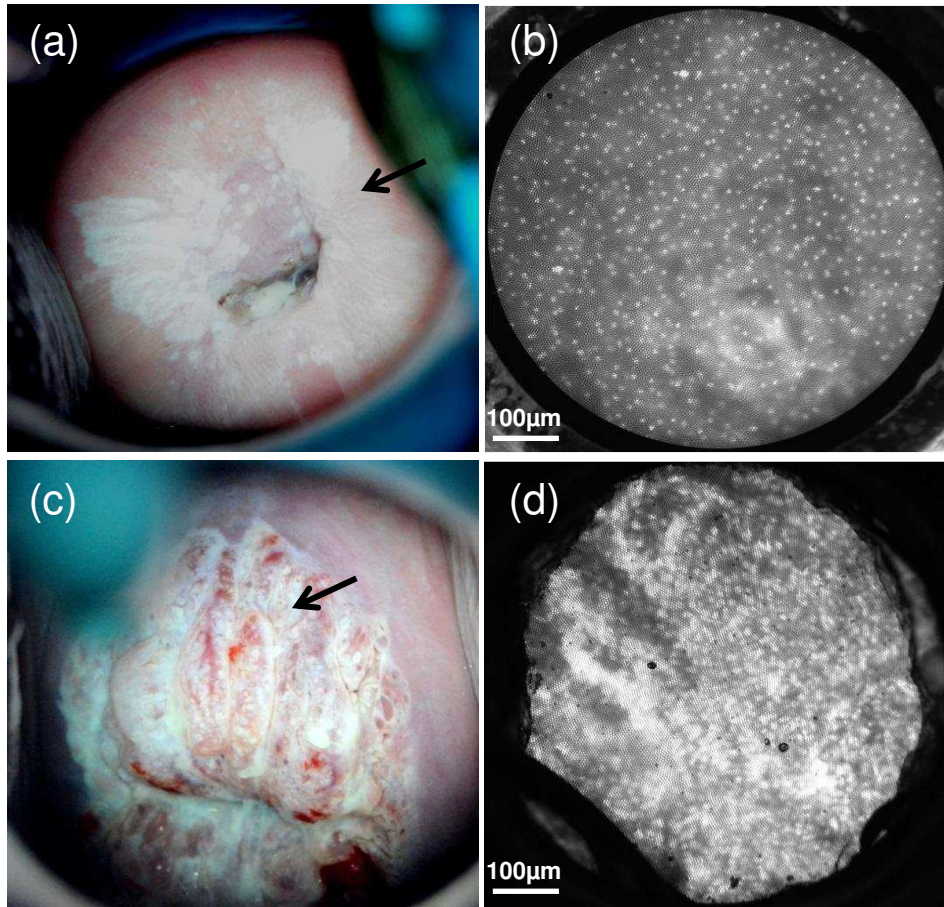


Figure 15: Typical colposcopic and HRME images. The top row illustrates images obtained from a clinically normal region of the cervix. (a) The black arrow in the colposcopic image indicates the area imaged with the HRME. (b) The HRME image shows small, uniformly spaced nuclei, consistent with the histopathology diagnosis of pathologic changes. The bottom row shows images from a clinically abnormal region of the cervix. (c) The black arrow in the colposcopic image indicates a region with a clinical impression of high grade disease imaged by HRME. (d) The HRME image shows large, pleomorphic, crowded nuclei, and was consistent with the histopathology diagnosis of CIN 3.

4.3 RESULTS

A total of 128 unique sites from 60 subjects were imaged and biopsied. Images from 13 of these sites failed the quality control as described above. Images from another thirteen sites were not included because they were acquired from columnar epithelium, and 3 sites were discarded because of inconclusive pathology diagnosis. The remaining 99 sites were grouped according to histopathology diagnosis (Table2).

Figure 15 shows representative colposcopic images and HRME images from two patients in the study. The top row (a, b) illustrates images obtained from a clinically normal region of the cervix. The black arrow in the colposcopic image indicates the area imaged with the HRME. The resulting HRME image shows small, bright nuclei with dark cytoplasm and relatively large and evenly spaced internuclear separation, which is consistent with the histopathology diagnosis of normal. In contrast, images of a clinically suspicious site are shown in the bottom row (c, d). The black arrow in the colposcopic image indicates a clinically suspicious region with a thick aceto-white lesion where the HRME image was acquired. The resulting HRME image shows a remarkable increase in nuclear-to-cytoplasmic ratio and crowding of nuclei. This site was diagnosed as CIN 3 by histopathology.

Figure 16a shows a scatter plot of the previously published nuclear-to-cytoplasmic ratio calculated from the training set [111]. The horizontal dashed line represents the discrimination threshold at 0.163 determined in the previous study. Figure 16b shows a scatter plot of the nuclear-to-cytoplasmic ratio calculated from each of the 99 sites imaged in this validation study. The horizontal dashed line indicated the same threshold used for the training set. Figure 17 shows the corresponding receiver operator characteristic curves. At the same threshold as in Figure 16, the algorithm yields sensitivities and specificities of 86% and 87% for the training set and 90% and 85% for the validation set, respectively. The sensitivity and specificity of clinical impression for the validation set for the same sites were 55% and 88%, respectively.

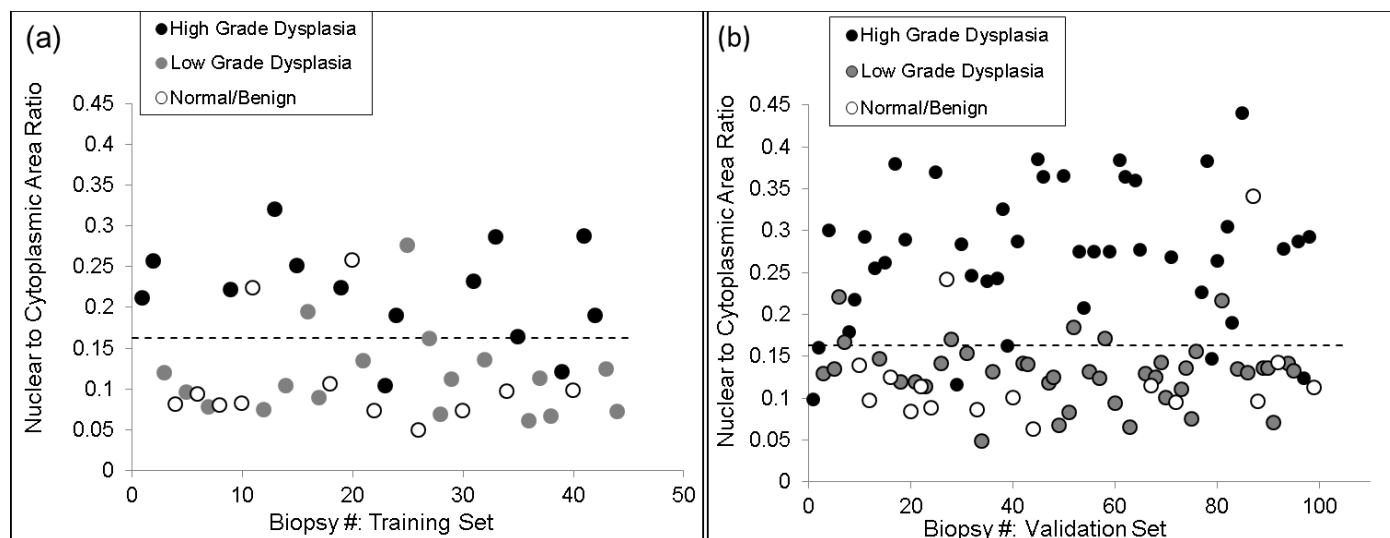


Figure 16: Scatter plot of N/C ratio for sites in the training and validation sets, broken down by histopathologic diagnosis. (a) N/C ratio of the 44 sites in the training set (previously published in [16]). (b) N/C ratio of the 99 sites in the validation set. The horizontal dashed line in (a) indicates the discrimination threshold; sites with an N/C ratio >0.163 were diagnosed as neoplastic. This threshold yields a sensitivity of 86% and a specificity of 87% relative to the gold standard of histology. The same threshold was applied to the validation set and yielded a sensitivity of 90% and specificity 85% relative to histology.

4.4 DISCUSSION

The purpose of this study was to assess the reliability and reproducibility of a previously developed image analysis algorithm to determine whether sites imaged with a high resolution microendoscope are neoplastic or non-neoplastic. In vivo digital images of the cervix were acquired from 128 unique sites in 60 patients. As in the previously acquired training set, images from tissue with high-grade precancer exhibited higher N/C ratio than benign tissue or tissue with low-grade precancer. Images could be accurately classified by simply calculating the N/C ratio and using a simple threshold; in this validation set, the algorithm discriminated between neoplastic and non-neoplastic tissue with a sensitivity of 90% and specificity of 85%. These results are very comparable to those that we previously reported in the training set [111]. In both cases, automated analysis of HRME images results in significantly better sensitivity than that of clinical impression.

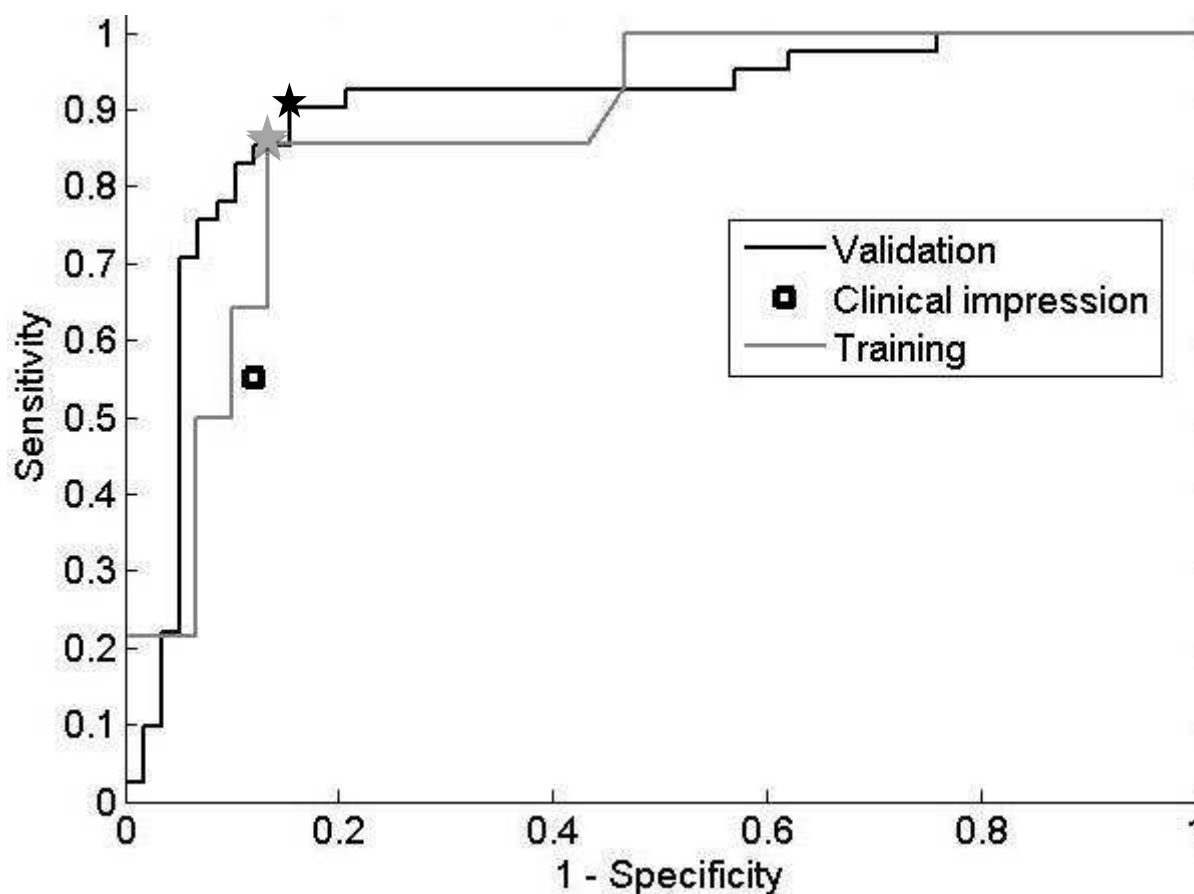


Figure 17: Receiver operator characteristic curve for the algorithm shown in Figure 2. The grey curve represents the training set; the Q-point corresponds to a sensitivity of 86% and a specificity of 87%. The black curve represents the validation set; the Q-point corresponds to a sensitivity of 90% and a specificity of 85%. The sensitivity and specificity of clinical colposcopic impression for the validation set for the same sites were 55% and 88%, respectively.

The findings of this study suggest that HRME imaging may have potential to improve real-time, noninvasive assessment of cervical pre-cancer in low-resource countries. HRME images can be acquired and interpreted at point-of-care, potentially reducing the cost and infrastructure needed to take, process, and read biopsies. In addition, see-and-treat programs are limited by the low specificity of HPV tests or VIA. The high specificity of HRME imaging

presents an opportunity to address these limitations; it may be combined with these tests to enhance the see-and-treat programs.

Our study has a number of limitations. First, the small field-of-view of the HRME makes surveillance of the entire cervix impractical. The device could be used in conjunction wide-field imaging systems to rapidly image the entire cervix and identify regions which are suspicious for neoplasia, and can then be interrogated using the HRME to confirm the presence or absence of neoplasia. Second, we excluded thirteen images from this study because they were acquired from columnar epithelium. Further improvements are needed to the image analysis algorithm to analyze images of columnar epithelium.

In summary, we have developed a low-cost, portable high-resolution imaging device capable of accessing indicators observed during pathological analysis such as cell morphology without the need for biopsy. Coupled with simple quantitative image analysis, the HRME has the potential to be used to improve cervical cancer screening, especially in low-resource settings.

5. MULTIMODAL DIGITAL IMAGER FOR THE DETECTION OF CERVICAL NEOPLASIA IN LOW-RESOURCE SETTINGS

5.1. Introduction

Cervical cancer continues to be a major health problem among women in developing countries. More than 85% of cervical cancer deaths occur in developing countries [1], where screening tools that allow detection of precancerous and early stage cervical cancer are unavailable or inadequate [113, 114]. In 2008, there were estimated 234,000 deaths in developing countries due to cervical cancer compared to just over 41,000 deaths in developed countries [1]. In developed countries, organized screening tests such as the Papanicolaou smear (Pap smear) test have enabled precancerous lesions to be diagnosed and treated early, subsequently reducing new cervical cancer cases and mortality rates. However, health care systems in many developing countries do not support Pap smear test or other types of screening tests. To be effective, these screening programs require relatively high-level infrastructure and well-trained personnel.

In the last three decades, researchers have embarked on finding screening alternatives appropriate for low-resource settings. Today, the single most widely available screening method in developing countries for the single visit approach is VIA (visual inspection with acetic acid). This is a simple visual test, where the cervix is examined with the naked eye before and after application of 3 to 5% acetic acid. Suspicious areas undergo “aceteowhitening”, meaning the lesions turn white in comparison to healthy tissue. VIA is inexpensive, requires minimal infrastructure, and allows for immediate treatment, eliminating the need for a laboratory. VIA has shown promising results in differentiating normal or low-grade dysplasia from high-grade dysplasia or invasive carcinomas [7, 31, 41, 43, 97, 115]. Another approach based on visual inspection, VILI (Visual Inspection with Lugol’s Iodine) has also been explored. In a

multicenter study VILI presented improved sensitivity over VIA while maintaining similar specificity [43].

Other techniques investigated include HPV DNA testing. HPV DNA testing has shown promising results when complementing cytology in primary screening [32, 33]. Some studies presented sensitivity and specificity of HPV DNA varying from 65% to 95% and 70% to 96% respectively [7]. These results suggest that HPV testing may be considered for primary cervical cancer screening in low-resource settings since it is easier to implement than cytology screening. Although it is anticipated that HPV DNA testing may reduce costs associated with unnecessary colposcopy, the currently available HPV tests are still relatively expensive to be fully implemented in low-resource settings; due to the need for laboratory infrastructure for processing. Also, currently available HPV tests require six hours to produce results, resulting in multiple clinic visits for screening and treatment. More recently, a rapid HPV test (careHPV) has been developed and promises to offer potential solutions to the limitations associated to the currently available HPV tests [35]. However, low specificity was reported, limiting the efficacy of see-and-treat programs.

A number of optical techniques have recently been investigated as alternative detection methods in developing countries. Optical imaging has the capability to obtain and display wide-field images of epithelial tissues in real-time [44]. Wide-field imaging systems enable a relatively large field of view (50-100 mm) to be visualized at moderate resolution under conventional white-light illumination, as well as in fluorescence and polarized light modes [62, 63]. Supplementing conventional imaging with the use of polarized light, narrowband reflectance, and/or fluorescence imaging modes has been shown to improve sensitivity and

specificity for several types of cancer, by reducing specular glare, enhancing vascular contrast, and detecting alterations in tissue fluorescence associated with the presence of disease.

Orfanoudaki et al. evaluated a wide-field, multispectral reflectance imaging system in a study involving 123 women. The system improved the diagnosis as the false positive-diagnostic rate was found to be 1.7%, compared to 22% and 24.4% of conventional colposcopy and Pap test respectively [68]. The United States Food and Drug Administration (FDA) in 2006 approved a trimodal imaging system called; LUMATM. LUMATM uses a 337nm UV nitrogen laser for fluorescence and two xenon flash lamps for reflectance. This system was evaluated in two prospective, randomized controlled studies, yielding higher sensitivities when compared to that of colposcopy [65, 70]. We previously developed a Multispectral Digital Colposcope MDC to measure multispectral autofluorescence and reflectance images of the cervix [62]. The MDC is a modified standard colposcope with the ability to measure reflectance and fluorescence images. Two excitation wavelengths, 330 and 440nm showed the greatest diagnostic power relative to histology [32]. In a different study, the MDC achieved a sensitivity of 79% and specificity of 88% in distinguishing high-grade precancer from low-grade precancer or normal tissue [63]. These wide-field imaging devices have shown promising results for detecting abnormalities in the cervix; however, their use has been limited to medical facilities in developed countries due to their complexity, limited portability and high cost.

In this study we present a portable, less complex, battery-powered, and robust wide-field system capable of operating in both fluorescence and reflectance. The multimodal digital imager (MDI) is based on similar principles to the devices that were previously developed in our lab [71, 73], but was specifically designed to image the cervix. Table 3 shows the design criteria and the

actual performance of the MDI. The system includes three imaging modes: cross-polarization reflectance (to reduce specular reflection), narrowband green reflectance (to improve contrast of the vasculature), and fluorescence imaging using proflavine as a contrast agent.

In low-resource areas where highly trained clinicians may not be available, automated algorithms to distinguish precancer from normal are very important to help healthcare providers with the diagnosis. Automated analysis techniques have the potential to reduce subjectivity and enhance reliability and reproducibility of the diagnosis. In this study computer-aided image analysis is also presented and its diagnostic performance reported. We investigated image parameters that have been previously found to correlate with diagnosis. These include average RGB pixel intensity values, the standard deviation of RGB pixel values, and ratios of the average RGB pixel values [62, 116 – 119].

	Design criteria	Performance of the MDI
Imaging modes	<ul style="list-style-type: none"> - Cross polarized reflectance - Narrow band green reflectance - Fluorescence 	<ul style="list-style-type: none"> - Cross polarized reflectance - Narrow band green reflectance - Fluorescence
Size	Compact (fit inside a backpack)	6 x 4 x 6 inches
Weight	<10 lbs.	4 lbs.
Power supply	Battery powered	Battery powered
Resolution	50 μm to 100 μm	88.3 μm
Field of view	35 - 60 mm	55 mm
Working distance	250 – 300 mm	250 mm
Approximate cost	<\$5K	\$3,500 (laptop excluded)

Table 3. Design criteria and performance of the MDI.

5.2 Materials and Methods

5.2.1 Instrumentation

A schematic diagram of the multimodal digital imager (MDI) is shown in **Fig. 18**. The MDI incorporates a white LED (MWWHL3, Thorlabs) for illumination, narrowband excitation filter (Semrock-550/49nm, Semrock), fluorescence excitation filter (Semrock-445/25nm, Semrock), illumination polarizer (Chroma-21003a, Chroma), fluorescence emission filter (Semrock-550/88nm, Chroma), observation polarizer (Chroma-21003a, Chroma), and CCD camera (GRAS-14S5C-C, Point Grey Research). Light from the LED is collimated by a 10 mm focal length lens, passes through the narrowband filter, polarizer or fluorescence filter depending on the imaging mode; another 50 mm focal length lens is then used to illuminate the entire cervix tissue. The illuminated field of view (FOV) is 55 mm in diameter at a working distance (WD) of 250 mm. Light emitted from the tissue is collected and directed through either a fluorescence emission filter or a polarizer depending on the imaging mode. A 25 mm focal length macro lens (M118FM25 Megapixel, Tamron) is used to image the light onto a CCD camera. The polarizers, excitation and emission filters are mounted on a motorized filter wheel. The entire system is controlled by a custom LabView graphical interface (Austin, Texas), and images are stored as JPEG files for later review and processing.

The MDI specifications are listed in Table 3. The resolution of the MDI was measured to be 88.3 μm , which is within the acceptable range (50-100 μm) specified. This is particularly important because the system with a resolution exceeding 100 μm might fail to reveal changes in vascular atypia. The MDI weighs about 4 lb., measures 6 x 4 x 6 inches, and is powered by a rechargeable battery. The total cost of the MDI is approximately \$3500, excluding the cost of the

laptop. Optical standards, including positive and negative reflectance standards, positive fluorescence slides, and a frosted quartz disk to serve as a negative fluorescent standard were used to quantify the performance of the MDI as well as to track any changes occurring in the device over time. For white light illumination, color balance was achieved by imaging a white balance sheet and adjusting the RGB ratio in software so that equal pixel intensity values were obtained in the red, green, and blue channels. The fluorescence color slides were used as a standard to track any changes in color response or sensitivity of the camera over time in fluorescence mode. To confirm that there was no excitation leakage through the emission filter, the frosted quartz disk was imaged in fluorescence mode at exposure times and gain settings matching or exceeding those used for normal oral (lower lip) tissue fluorescence imaging. Signal from the negative control was less than 5% of that associated with tissue from a normal volunteer.

In order to assess the degree to which application of proflavine increases the fluorescence intensity of normal mucosal tissue, the inner lip of two normal volunteers was imaged after application of 0.01% proflavine. The proflavine fluorescence to autofluorescence ratio was found to be approximately 5.5.

5.2.2 In vivo pilot study

In order to determine the feasibility of using this optical system in low-resource areas, the MDI was tested in Botswana as a pilot clinical study. The Institutional Review Board at Rice University and the Health Research Division Office of the Botswana Ministry of Health approved the study protocol. Written informed consent documents were available in both English and the local national language (Setswana). All patients involved in the study were given written

informed consent. Patients at least 18 years of age with an abnormal Pap smear referred for colposcopy and who were not pregnant were eligible to participate in the study.

Following application of 3% acetic acid the cervix was first examined by routine colposcopy. Abnormal cervical lesions were identified and noted by the study physician. The study physician described and classified each lesion as clinically high grade, clinically low grade, or clinically normal. Following colposcopic examination, the MDI was then advanced and several images were captured in cross-polarized white-light mode followed by narrow band green mode. Proflavine (0.01% w/v in sterile phosphate buffered saline) was then topically applied to the cervix, and MDI fluorescence images were recorded. Following fluorescence imaging, Lugol's iodine was applied to the cervix and colposcopic images were recorded. The MDI was reintroduced again to collect several post Lugol's iodine images.

Diagnostic Category	Histopathology Diagnosis	Number of Sites Imaged
Normal/Benign	Normal	7
	Inflammation	7
Low Grade Dysplasia	HPV Effect	10
	CIN 1	7
High Grade Dysplasia	CIN 2	2
	CIN3	12
	TOTAL	45

Table 4. Distribution of sites imaged by MDI, grouped according to histopathology diagnosis

Immediately after optical measurements, a clinically normal site was biopsied in addition to up to 2 abnormal/ suspicious sites and then submitted for histopathologic diagnosis. Diagnostic classification categories included normal, inflammation, HPV effect, grade 1 cervical intraepithelial neoplasia (CIN 1), grade 2 cervical intraepithelial neoplasia (CIN 2), and grade 3 cervical intraepithelial neoplasia (CIN 3). CIN2 and CIN3 (high grade dysplasia) were categorized as neoplastic tissue and all others were categorized as non-neoplastic.

5.2.3 Data processing

All digital images acquired with the MDI were stored as JPEG files on the computer and were later reviewed for quality control by a reviewer blinded to all diagnostic information. Images were discarded if they were out of focus or the biopsied site was not visible. All images which passed quality control and had a corresponding histopathologic diagnosis were analyzed with image analysis software (Matlab R2010b) to automatically extract quantitative parameters. Although narrow band green and fluorescence images were acquired, these images were not used in this study as we believed the acetowhitened and post Lugol's iodine images to be more useful for the current analysis.

Quantitative analysis began with selection of a region-of-interest (ROI) that matched the size of a biopsy specimen from each image. From each ROI of the post-acetic acid images, features calculated included raw red, green, blue (RGB) pixel intensity values, and the relative contribution of R, B, G (i.e. $R/(R+G+B)$, $G/(R+G+B)$, $B/(R+G+B)$). These features have been previously quantified and reported to correlate with diagnosis [11, 18]. From each ROI of the post-Lugol's iodine image, the following images features were calculated: RGB pixel intensity values, CYM (cyan, magenta, yellow and key) pixel intensity values from the CMYK color

model, and HSV (hue, saturation, and value) pixel intensity values from the HSV color model. Finally, only two features from this list were selected as potentially useful for classification: relative red pixel intensity for the post-acetic acid images and hue pixel intensity values for the post-Lugol's iodine images.

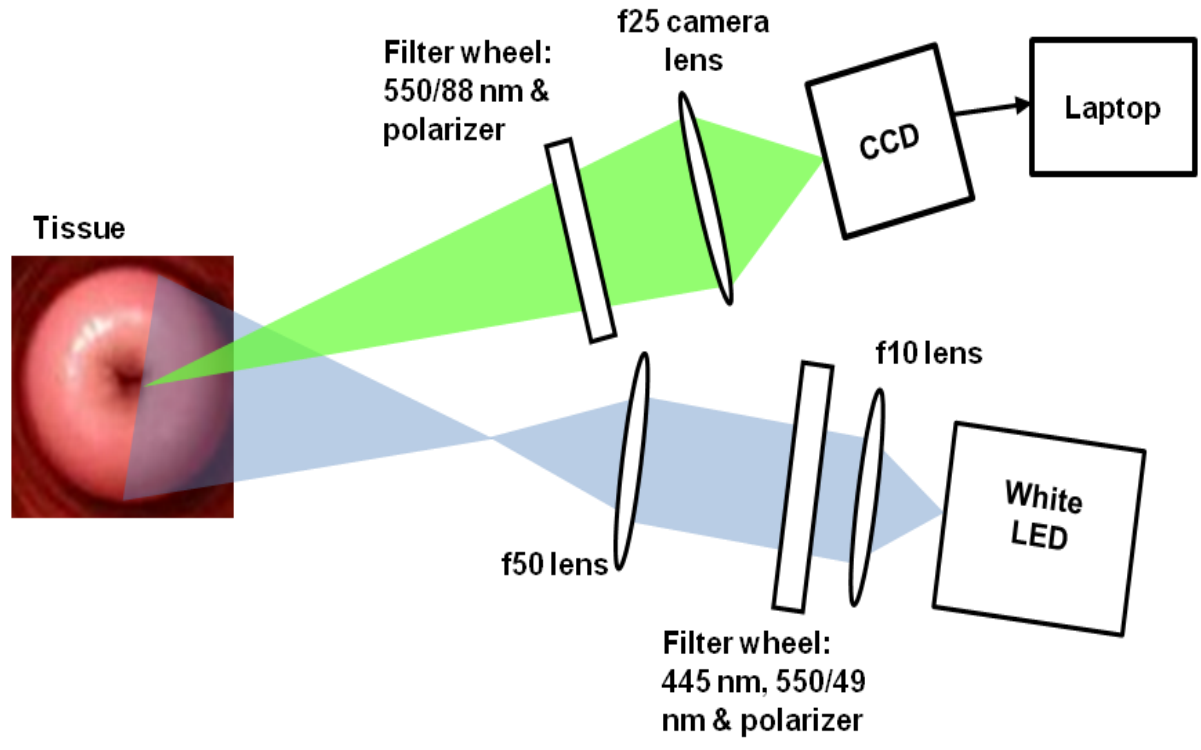


Figure 18. Schematic diagram of the Multimodal Digital Imager (MDI)

- Abbreviations:**
LED: Light-emitting diode
CCD: Charge-coupled device (camera)

5.3 Results

MDI images were acquired from 60 unique sites in 30 patients. Out of these, 8 sites were discarded due to lack of pathology diagnosis. Seven more sites were left out because biopsy sites were not visible on the acquired images. Table 4 summarizes the histopathologic diagnoses of the remaining 45 sites in 23 patients.

Figure 19 shows images of the cervix from two patients obtained using the multimodal optical imager. The top row shows images from patient A. A black arrow (1) in the post-acetic acid image indicates an area of aceto-whitening lesion that was confirmed to be HPV effect (low grade and non-neoplastic) by histopathology. Arrow (2) indicates an area of normal cervical tissue which presents pinkish/reddish in color. In comparison, the post-Lugol's iodine image shows a yellowish area (corresponding to arrow 1) and a brownish area (corresponding to arrow 2). The bottom row shows images from a patient with clinically apparent lesions (patient B). A thick aceto-white lesion is evident in the post-acetic image as indicated by the black arrow (1) and a thick mustard yellow of the corresponding area in the post-Lugol's iodine image. The histopathology report confirmed this area as neoplastic (CIN3). The black arrow (2) represents an area of normal cervical tissue. The lesion in patient B is thicker and slightly raised compared to the lesion in patient A.

For each of the 45 measured and biopsied sites, relative red pixel intensity in the post acetic acid images and mean pixel intensity of hue channel in post Lugol's iodine images were calculated. Figure 20 shows scatter plots of this analysis for each of the 45 measurement sites, grouped according to histopathology. Figure 20a shows the mean intensity of relative red for each measured site. A threshold value of 0.41 (shown as a dashed line in Fig. 20a) correctly classified non-neoplastic (normal/benign or low grade dysplasia) and neoplastic (high grade dysplasia)

sites with a sensitivity of 86% and specificity of 71%. Figure 20b shows values of the mean pixel intensity of hue channel at the same sites as Fig. 20a. A threshold value of 0.05 correctly classified these measured sites into the same categories as described for mean intensity of relative red with a sensitivity of 86% and specificity of 51%.

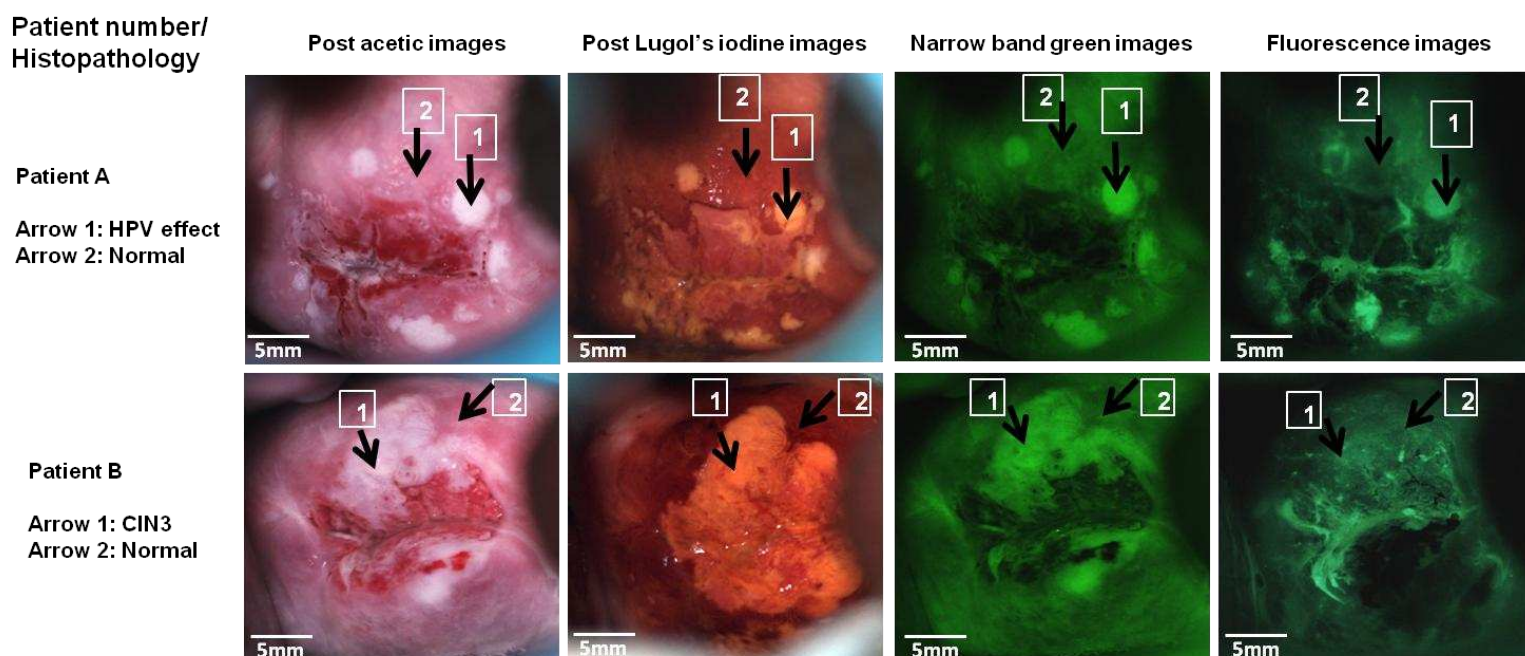


Figure 19: Images of the cervix from two patients obtained with the multimodal optical imager: (1st column) post acetic images, (2nd column) post Lugol's iodine images, (3rd column) narrow band green images, and (4th column) fluorescence images. Arrows indicate region-of-interest; (1) abnormal/suspicious and (2) normal.

Figure 21 shows the receiver operator characteristic (ROC) curve for a diagnostic algorithm, which combines the parameters derived in Figure 20. The Q-point indicated on the figure corresponds to a sensitivity of 86% and specificity of 74%. A combination of these features improved the specificity of each individual feature when used alone. For comparison, the sensitivity and specificity of clinical impression for the same sites were 57% and 84%, respectively.

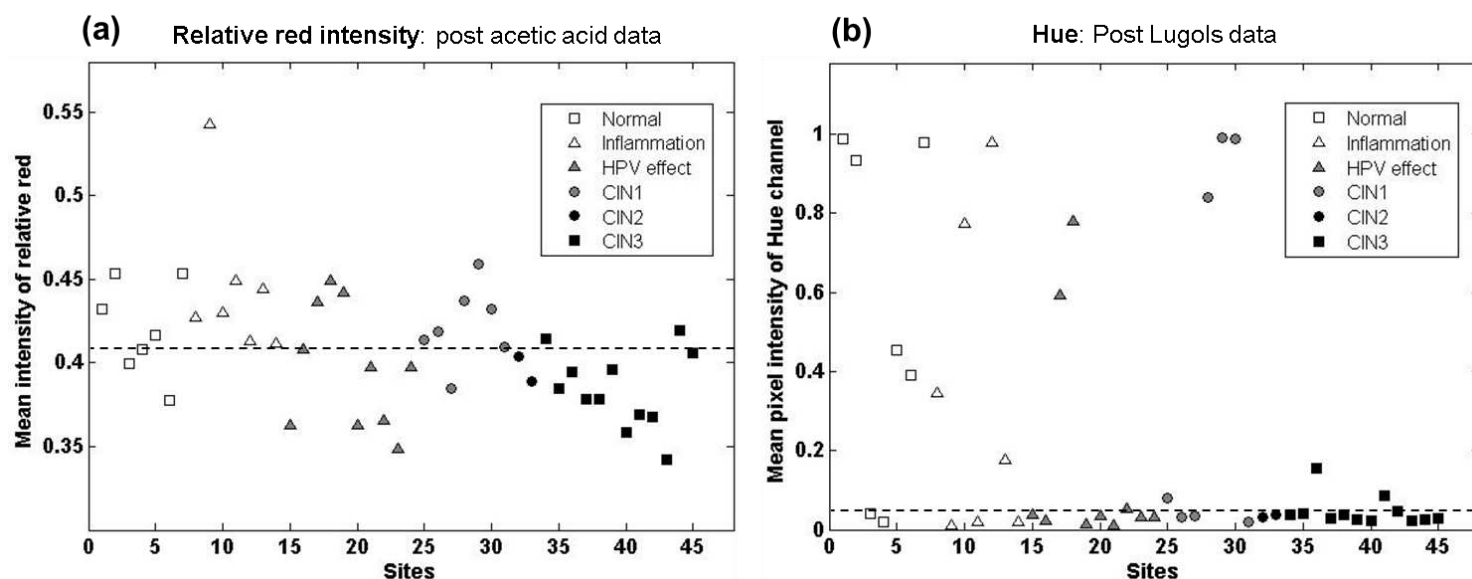


Figure 20: Quantification of post acetic acid and post Lugol's iodine images, broken down by histopathologic diagnosis. (a) Mean relative red intensity at each of the 45 sites measured in the study. (b) Mean pixel intensity of Hue channel for the same 45 sites shown in (a). Dashed lines represent linear threshold values to discriminate between normal/benign/low grade dysplasia sites, and those with high grade dysplasia. For (a) a sensitivity of 86% and a specificity of 71% for separating samples diagnosed as high grade dysplasia from samples diagnosed as low grade dysplasia or normal/benign were measured whereas for (b) a sensitivity of 86% and a specificity of 51% were measured.

5.4 Discussion

This pilot study demonstrates the use of a low-cost, portable, multimodal optical imager that has the potential to improve cervical cancer screening in low-resource settings. The device is battery powered, incorporates LED illumination, and is capable of three imaging modes. Data from 23 study subjects were analyzed to determine which imaging modalities provide the greatest optical contrast, and to determine if objective classification algorithms could be used to aid in identifying lesions in the cervix. In low-resource areas where knowledgeable manpower is limited, automated algorithms to distinguish precancer from normal tissue are important to help clinicians make an accurate diagnosis. Two features were selected as potentially useful for classification: 1) relative red pixel intensity for post acetic acid images and 2) hue pixel intensity

values for post Lugol's iodine images. Relative red pixel intensity resulted in better classification performance with a sensitivity of 86% and specificity of 71%. Hue pixel intensity yielded the same sensitivity but a low specificity of 51%. The low specificity in the hue pixel intensity may be attributed to the presence of HPV infection, which tended to produce false positive images (yellowish staining). However, when these two features were used in combination, the specificity was better than that of each feature. This demonstrates the potential of incorporating multiple imaging modes.

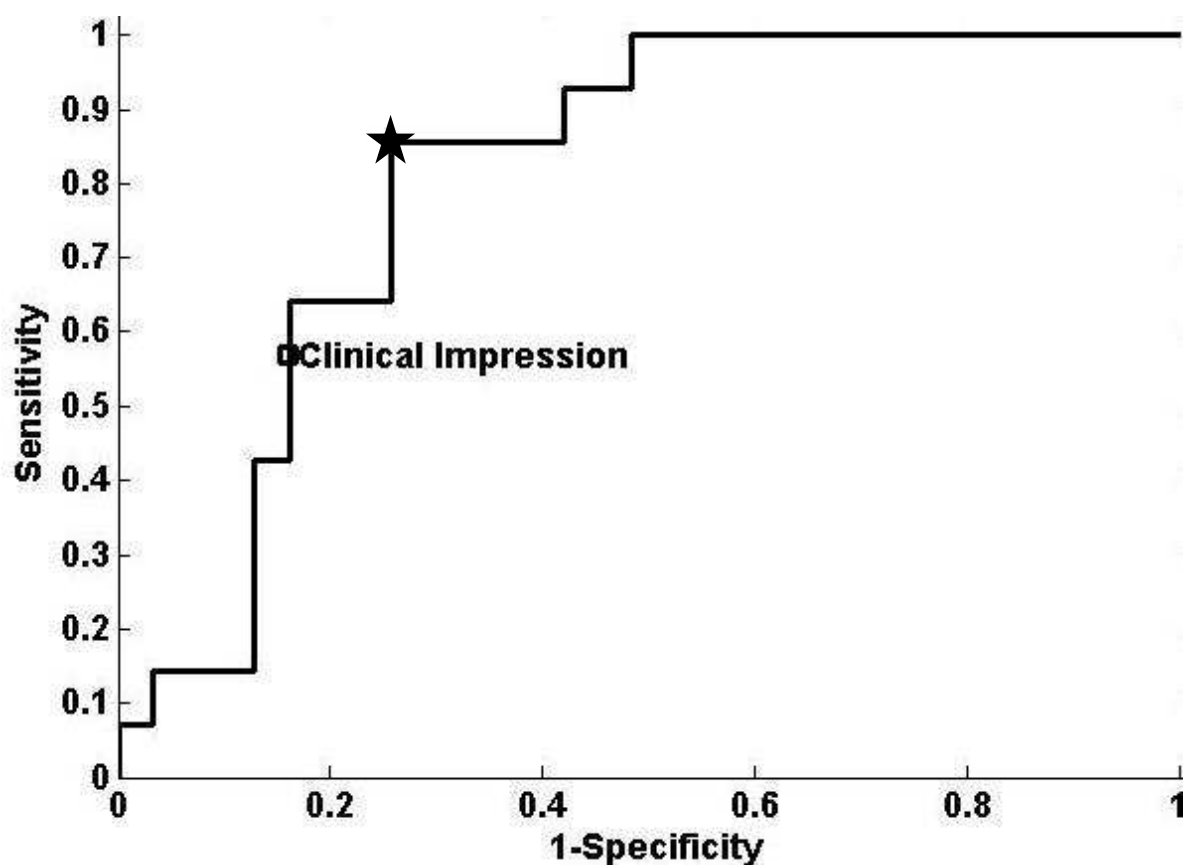


Figure 21: Classification of measured sites using both post acetic acid and post Lugol's iodine. Receiver operator characteristic curve for the features in Figure 3. The star indicates the Q-point, with a sensitivity of 86% and a specificity of 74%. For comparison, the sensitivity and specificity of clinical colposcopic impression for the same sites were 57% and 84%, respectively.

These results are encouraging; however, some limitations exist. First, the study involved 45 sites from 23 patients. A larger study is required to evaluate the diagnostic performance of the device. Second, the study showed the low specificity. This may be addressed by using this system in combination a high-resolution optical imaging system such as the high-resolution microendoscope (HRME) [111]. Wide-field optical imaging system can highlight suspicious areas with high sensitivity, while high-resolution optical imaging system can confirm the presence of disease with high specificity. Last, more research is need to determine the potential of analyses of narrow band green and fluorescence images which were acquired by the MDI but were excluded in this analysis.

In conclusion, we have built a low cost, portable, multimodal optical imaging system and coupled it with quantitative image algorithms. Although further work is needed to address the limitations in this study, the results from this pilot study suggest that this simple imaging device can potentially improve cervical cancer screening efforts in low-resource settings where screening programs for early detection are either inadequate or unavailable.

Chapter 6: WIDE-FIELD MULTIMODAL IMAGING AND HIGH-RESOLUTION MICROENDOSCOPE IMAGING FOR DETECTION OF CERVICAL NEOPLASIA

6.1 Introduction

Cervical cancer is the 2nd leading cause of cancer death among women in the developing world [1]. Women in developing countries are at greater risk of developing or dying from cervical cancer, due to unavailability or inadequate screening tools [1]. In contrast, women in the developed world are at much lower risk of developing or dying from cervical cancer as they have access to screening for precancer and early cancer by cervical cytology (the Pap test), and/or human papillomavirus (HPV) DNA testing. An abnormal screening test is followed by examination of the cervix using colposcopy with directed biopsies to diagnostically confirm the presence of disease, and treatment of neoplastic lesions. [95]. Unfortunately, it is challenging to implement these proven screening and diagnostic tools in developing countries, due to lack of financial resources, infrastructure, and trained personnel.

Strategies such as visual inspection with acetic (VIA), visual inspection with Lugol's iodine (VILI) have been developed and explored in low-resource countries. VIA and VILI are easy to implement in a single clinic visit and they are relatively inexpensive. The sensitivity of VIA and VILI to detect cervical dysplasia and cancer in low-resource settings has been shown to be similar to standard colposcopy, however, with a markedly lower specificity [38, 41, 107, 120]. Apart from low specificity, these tests are subjective; accuracy varies from one health-care provider to the other.

HPV DNA testing has also been studied as a primary screening test for cervical cancer in developing countries [96, 122]. Although, promising results have been reported in these studies,

currently available HPV tests pose several additional challenges for low-resource settings. They are expensive, require laboratory infrastructure for processing, and need a waiting time of one or more days for results. A rapid-result HPV test (careHPV) which is currently in development is lower in cost and provides results within a few hours; however, low specificity has been reported [35]. Indeed, current see-and-treat programs are limited by the low specificity of HPV testing, VIA or VILI. There is an important need for affordable and effective tools to improve early detection of cervical precancer in low-resource settings.

Optical imaging has emerged as a promising technique to improve detection of cervical neoplasia [76]. High performance optical imaging systems can be constructed at relatively low cost, and image analysis can be automated; thus, these technologies may provide a way to bridge the gap of cervical cancer screening for developing countries. Wide-field optical imaging systems can be used to acquire macroscopic images of the entire cervix, highlighting suspicious areas with high sensitivity [12, 63, 68]. High-resolution optical imaging systems can acquire microscopic images [45, 56, 79, 111], confirming the presence of disease with high specificity. The use of contrast agents with these systems can enhance image contrast, thus highlighting changes in biomarkers of cervical neoplasia [44].

We hypothesized that a combination of wide-field and high-resolution optical imaging of the cervix could assist in the detection of cervical neoplasia and that these techniques could be implemented effectively in low-resource settings. In this study, wide-field imaging and high-resolution microendoscopy were performed with patients undergoing colposcopic evaluation for cervical cancer or pre-cancer at the women's clinic at Princess Marina Hospital in Botswana.

Quantitative image analysis was used to develop a classification algorithm; sites determined to be positive by wide-field imaging were further classified by high-resolution microendoscopy.

6.2 Materials and Methods

6.2.1 Study population

The study protocol was reviewed and approved by the Institutional Review Boards of the Health Research Division Office of the Botswana Ministry of Health and Rice University. Patients who were over 18 years of age, were not pregnant, and scheduled colposcopic assessment because of an abnormal Pap smear result were recruited to the study. All participating subjects received and signed a written informed consent document which was available in both English and the local national language (Setswana).

6.2.2 Imaging systems

A wide-field imaging system was originally designed for cross-polarized and fluorescence imaging; here, we used the system only for cross-polarized imaging. The main components of the system for cross-polarized imaging include a white light LED (MC-E, Cree, Durham, NC), a macro lens (AF Micro-Nikon 105 mm, Nikon, Tokyo, Japan), and a digital camera (D7000, Nikon, Tokyo, Japan) as shown in Figure 22a. Cross-polarized imaging was implemented using a polarizing beam splitter (48-545, Edmunds Optics, Barrington, NJ). The polarizing beam splitter directs linearly polarized white light to the sample; light reemitted from the sample orthogonal polarization is then transmitted via the polarizing beam splitter to a detector. The size of the illumination field is 50 mm in diameter at a working distance of 300 mm. Light was collected through a Dichroic mirror and a 435 nm longpass filter (Chroma,

HQ435LP) included in the system to enable fluorescence imaging. An image of the sample is visualized on the LCD screen of the camera in real-time. The spatial resolution of the system was measured to be 79 μm . The entire system weighs 5.6 pounds and is powered by a rechargeable battery.

A high-resolution microendoscope (HRME) system capable of obtaining images with subcellular resolution has been previously described [Muldoon, Pierce JOVE]. Briefly, the HRME consists of an LED at a wavelength peak of 455 nm for illumination (M455L2, Thorlabs, Newton, NJ), a fiber bundle (FIGH-30-850N, Fujikura, Tokyo, Japan), a 10X NA objective lens (RMS10X, Thorlabs, Newton, NJ), and a CCD camera (GRAS-14S5M, Point Grey, Richmond, Canada). Light from the LED is directed through the fiber bundle to the surface of the tissue. Fluorescence emission from the tissue travels through the same fiber bundle and is imaged onto a CCD camera as shown in Figure 22b. The probe used in the current study provides a 720 μm diameter field-of-view with 4.4 μm spatial resolution.

	Histopathology diagnosis	No. of site	Clinical impression			Combined classification analysis		
			No. sites normal	of sites abnormal	% accuracy	No. sites negative	of sites positive	% accuracy
Non-neoplastic	Normal	11	10	1	91	10	1	91
	Inflammation	13	13	0	100	11	2	85
	HPV effect	38	27	11	71	31	17	82
	CIN 1	11	7	4	64	10	1	91
Neoplastic	CIN 2	8	5	3	38	4	4	50
	CIN 3	37	11	26	70	4	33	89
	Total	118						

Table 5. Histopathology diagnosis vs. clinical impression, and vs. imaging accuracy of the measured sites

6.2.3 Study procedure

All subjects underwent routine colposcopic examination following application of 3% acetic acid. The study physician identified, described and classified each lesion as clinically high grade, clinically low grade, or clinically normal. Following colposcopic examination, several cross polarized white light images of the cervix were captured using the wide-field imaging system. Each image was acquired with a 12 ms integration time and ISO 6400. Next, proflavine (0.01% w/v in sterile phosphate buffered saline) was applied topically to the cervix using a cotton swab. Following application of proflavine, HRME images were recorded with the probe slightly touching the tissue at each site defined by the physician. Following HRME imaging, Lugol's iodine was applied to the cervix and colposcopic images recorded as part of the standard of care at Princess Marina Hospital. The wide-field system was then advanced to obtain cross polarized white light images. After all optical measurements, each site imaged was biopsied, including one site which appeared normal by clinical impression. Biopsy specimens were immediately sent for standard histologic analysis.

Diagnostic classification by a single expert pathologist included normal, inflammation, HPV effect, grade 1 cervical intraepithelial neoplasia (CIN 1), grade 2 cervical intraepithelial neoplasia (CIN 2), grade 3 cervical intraepithelial neoplasia (CIN 3), carcinoma in situ (CIS), and squamous cell carcinoma (SCC) using standard histopathologic criteria [35, 122]. For the purpose of this data analysis, CIN 2, CIN3, CIS and SCC were categorized as neoplastic and all others were categorized as non-neoplastic.

6.2.4 Image Analysis – WF Imaging

First, post-acetic acid and post-Lugol's images obtained with the wide-field imaging system underwent quality control assessment where by images were discarded if they appeared visually out of focus or a site biopsied was not visible. Regions of interest (ROI) were then selected from images which met the quality control criteria; the ROI were sized corresponding to biopsy specimens, which was 4 mm². Following ROI selection, the following image features were calculated from post acetic image to identify aceto-white epithelium: the raw red, green, blue (RGB) pixel intensity values, the cyan, yellow, magenta (CYM) pixel intensity values from the CMYK color model, and the relative contribution of R, B, G pixel to the total intensity [119]. For each post-Lugol's image, the following images features were calculated: RGB pixel intensity values, CYM pixel intensity values, and the hue, saturation, value (HSV) intensity values from the HSV color model.

6.2.5 Image Analysis – High-resolution Imaging (HRME)

Data were reviewed to ensure that the HRME images met quality control metrics. Images were discarded if more than 50% of the field of view seemed out of focus, if there was evidence of motion artifact, contained significant debris, or if it seemed that the fiber-optic probe was not in contact with the tissue. Selection of regions of interest within images, data processing, data analysis, and histopathologic correlation for the HRME were identical to those reported previously [111]. The nuclear-to-cytoplasmic area ratio (N/C ratio) was quantified by image analysis software (MATLAB, Natick, MA). The details of the software can be found here [111]. Briefly, the ROI was manually selected from each HRME image. Median filter was then

applied to the ROI to eliminate the fiber bundle patterns. Next, the image was converted to a binary image and a threshold applied to segment nuclei. Among the segmented nuclei, small objects assumed to be noise (<50 pixels) and large objects assumed to be clumps (>1500 pixels) were removed. Lastly, nuclear-to-cytoplasmic area (N/C) ratio was calculated by summing the number of pixels corresponding to nuclei and divided by the total number of pixels in the ROI. Nuclei appeared as bright dots on dark cytoplasm in each HRME image. The diagnostic classification algorithms and thresholds previously developed that study [111] were directly applied here to calculate the diagnostic performance of the HRME.

6.2.6 Image Classification

A two-step procedure was used to develop a classification algorithm to classify each measured site as neoplastic or non-neoplastic. In the first step, the image features extracted from both wide-field post-acetic acid images and post-Lugol's images were used to classify each ROI of the measured site as potentially neoplastic or non-neoplastic. We developed an algorithm using wide-field parameters for this purpose. The classifier based on a two-class linear discriminant analysis was used to classify the data using image features; features were added one at a time until performance did not improve further. The receiver operating characteristic (ROC) curve for the classifier was plotted for this step and the threshold was established on a point of the ROC curve by maximizing sensitivity so that any neoplastic sites would be less likely to be missed. In the second step, sites identified as potentially neoplastic by wide-field imaging were further evaluated with the high-resolution imaging parameter; the N/C ratio for HRME images was used to classify the sites as neoplastic or non-neoplastic using a previously developed algorithm [give reference]. Sites determined to be potentially non-neoplastic by wide-

field imaging were considered to be non-neoplastic for the classification algorithm and were not evaluated further. The same data were used to both train and validate the approach. Histopathologic diagnosis was used as gold standard.

6.3 Results

6.3.1 Subject information

A total of 90 patients were enrolled in this study. Five patients were excluded because images were not obtained due system malfunction and four patients were also excluded because biopsies were not taken. Images with corresponding pathology results were available from 167 sites in 81 patients. Out of these, thirteen sites were excluded because they were acquired columnar epithelium. The remaining images were reviewed using the QC criteria independently by three reviewers (TB, MKQ, and DS); 36 sites did not pass QC review. The resulting data set for further analysis consisted of images of 118 sites in 63 patients. Table 5 shows the histologic diagnosis for each measured site. According to histopathology (the gold standard), 73 sites were non-neoplastic (normal/ inflammation/ HPV effect/ CIN1) and 45 sites were neoplastic (CIN2/CIN3). In this study there were no cases of carcinoma in situ (CIS) or squamous cell carcinoma (SCC).

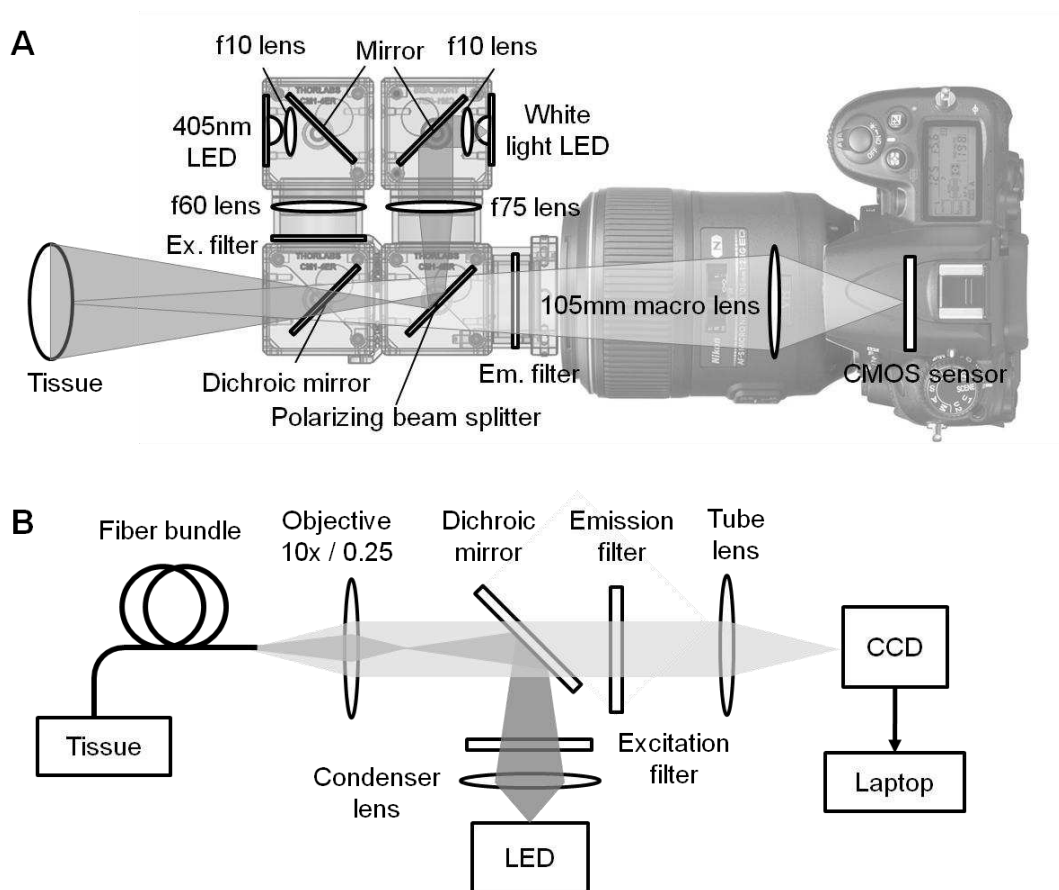


Figure 22. Schematic diagram of (a) the wide-field imaging system and (b) HRME

6.3.2 Combined analysis

Figure 23 shows wide-field and HRME images of sites that were correctly classified as non-neoplastic (a-c) and neoplastic (d-f) by both wide-field and high-resolution imaging. In the top row, a black circle indicates the ROI showing normal epithelium on a post-acetic acid image (a) and a white circle on a post-Lugol's image (b), which corresponds to the location of the HRME measurement. The corresponding HRME image (c) shows small, regularly spaced nuclei; the N/C ratio was calculated to be 0.09, which was consistent with the histopathologic diagnosis of normal. In the bottom row, a black circle indicates the site showing an abnormal aceto-white

lesion (d) and a white circle indicates an abnormal mustard yellow lesion (e). The corresponding HRME image (f) shows large, crowded, pleomorphic nuclei; the calculated N/C ratio is 0.27, which was consistent with the histopathologic diagnosis of CIN 3.

Figure 24 shows a site that was first incorrectly classified as neoplastic by both clinical impression and wide-field imaging, but correctly classified as non-neoplastic by HRME imaging. The site shows an aceto-white lesion and mustard yellow lesion on a post-acetic acid image and post-Lugol's image respectively but the calculated N/C ratio is 0.14, which consistent with non-neoplastic diagnosis by histopathology of HPV effect.

Figure 25a depicts a scatter plot of the hue intensity value of the post-Lugol's images for each measured site, which was found to be the single best performing feature for wide-field imaging. The decision line which classifies sites as potential neoplastic or non-neoplastic is shown, achieving a sensitivity and specificity were 91% and 58%, respectively. Figure 25b shows a scatter plot of the N/C ratio for sites determined to be positive by wide-field post-Lugol's imaging. The threshold value of 0.163 previously established here [111] was used to classify the sites as neoplastic or non-neoplastic, resulting in a sensitivity of 82% and a specificity of 85%. Table 5 summarizes accuracy of clinical impression and combined classification analysis versus histopathologic diagnosis.

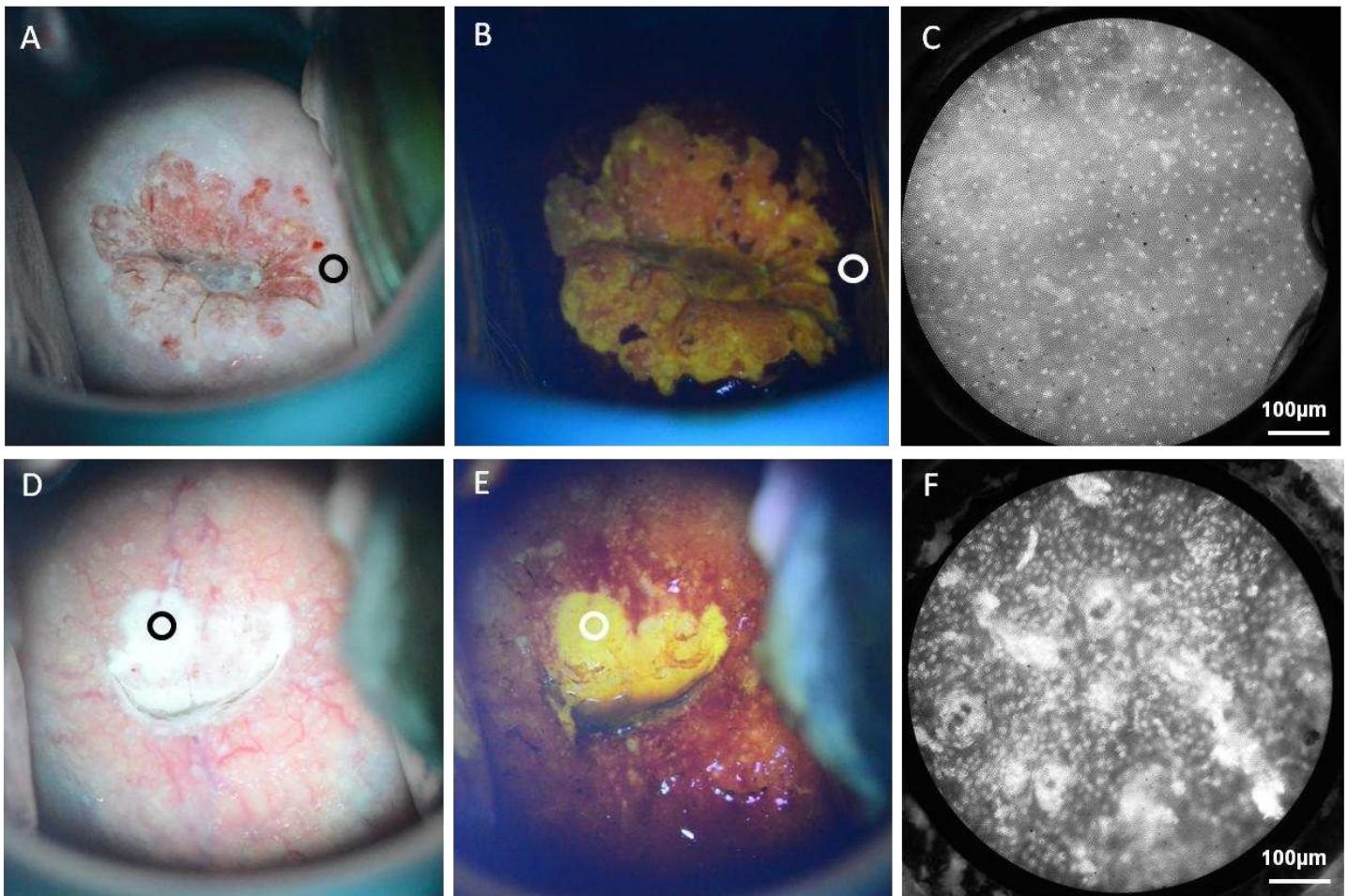


Figure 23. Multi-modal optical imaging of the cervix. (a-c) a site classified as True Negative by both wide-field imaging and HRME imaging. Clinical impression: normal. Histopathology: normal. (d-f) a site classified as True Positive by wide-field imaging and HRME imaging. Clinical impression: abnormal. Histopathology: CIN3. (a,d) Cross-polarized post-acetic acid images; a black circle shows a region of interest corresponding to location of HRME measurement, (b, e) cross-polarized post-Lugol's imaging; a white circle shows a corresponding region of interest. (C, f) HRME imaging.

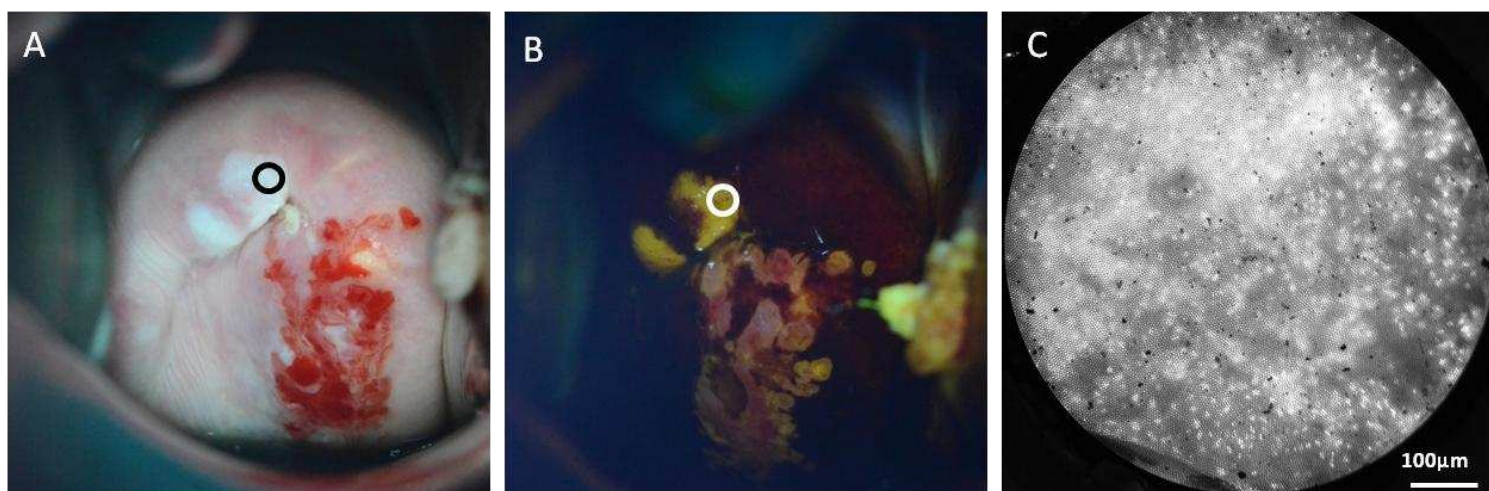


Figure 24. Site classified as False Positive by wide-field imaging, but True Negative by HRME imaging. Clinical impression: abnormal. Histopathology: HPV effect. (a) Cross-polarized post-acetic acid image; a black circle shows a region of interest corresponding to location of HRME measurement. (b) Cross-polarized post-Lugol's image; a white circle shows a region of interest corresponding to location of HRME measurement. (c) HRME image at the region of interest.

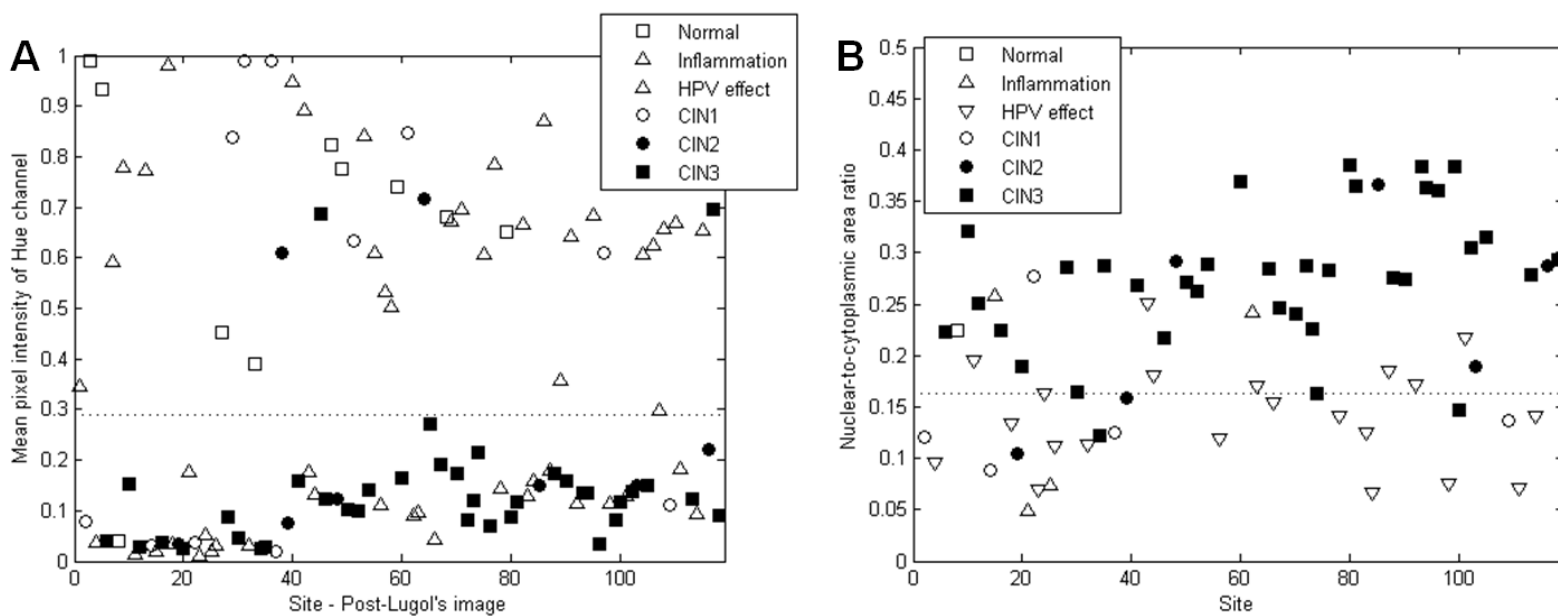


Figure 25. (a) Scatter plot of hue intensity value for each site imaged with wide-field post-Lugol's imaging. The decision line which classifies sites as neoplastic or non-neoplastic is shown. (b) Scatter plot of N/C ratio for sites determined to be positive by wide-field post Lugol's imaging and then imaged with the HRME. The decision line to classify sites as neoplastic or not using a threshold used for an independent HRME classification algorithm is shown.

6.4 Discussion

Wide-field post-Lugol's imaging has a high sensitivity for detecting cervical lesions, but may have difficulty in distinguishing precancer from benign lesions such as HPV effect. The use of high-resolution microendoscope in combination with wide-field imaging provides the ability to minimize errors of misclassifying non-neoplastic lesions for neoplastic lesions as demonstrated by figure 24. This raises the possibility of a combined measurement procedure in which wide-field imaging is used to identify suspicious lesions and guide the placement of the fiber bundle for HRME measurements.

In this study, wide-field imaging alone was found to have a sensitivity of 91% and specificity of 58%. The lower specificity may be attributed to the presence of HPV infection, which tended to incorrectly produce positive images (yellowish staining). The hue pixel intensity shown to misclassify HPV effect (non-neoplastic) as neoplastic.

The HRME was found to have a sensitivity and specificity of 84% and 84%, respectively. This can be compared to the HRME of a previous study including 44 sites in 24 patients, in which a sensitivity and specificity of 86% and 87%, respectively, were obtained [111], demonstrating reliability of the N/C ratio from the HRME images to distinguish neoplastic from neoplastic of the cervix.

The method of combining the wide-field imaging and high-resolution imaging results (the two-step procedure) gave a sensitivity of 82% and a specificity of 85%. Although the performance of the HRME imaging alone showed the results comparable or better than those of the combined analysis, wide-field imaging play an important role by guiding HRME probe placement. It might

be difficult to acquire HRME images without prior macroscopic examination. Given this situation, this combined analysis may be appropriate. These results are encouraging and may potentially impact cervical cancer screening in low-resource settings. The high specificity of the multimodal optical imaging results suggests that this platform could potentially lower the number of over-treated lesions associated with current screening tests, subsequently enhancing the “see-and-treat” programs currently in use in low resource settings.

While findings are encouraging, our study has a number of limitations. More research is needed to determine the potential of analyses of fluorescence images which were acquired by the wide-field system but were excluded in this analysis. This might provide additional useful information and improve diagnostic accuracy of the multimodal optical imaging. More combination methods such as maximum posterior probability, minimum posterior probability and/or mean posterior probability may be explored to maximize accuracy.

When combining data from wide-field imaging and high-resolution imaging, attention must be paid to registration of regions of interest within the wide-field image and sites measured with high-resolution system. It may be helpful if the measurement procedure includes the collection of images of the probe placed on the measurement site.

In summary, 118 sites in 63 patients were measured using both wide-field imaging and high-resolution microendoscope in a low-resource setting. Diagnostic algorithms and thresholds were established and applied to give quantitative analysis. Wide-field imaging alone was found to have a sensitivity and specificity of 91% and 58%, respectively. The combined analysis produced a sensitivity of 82% and a specificity of 85%. These results suggest that the overall

performance of noninvasive optical diagnostic methods may be enhanced through the use of platforms that combine both wide-field and high-resolution modalities.

Chapter 7: CONCLUSION

In summary, a number of clinical studies were performed in a low resource setting to evaluate the performance of wide-field imaging and high-resolution imaging. The performance of each technique was optimized individually and in combination, for noninvasive in vivo diagnosis of cervical neoplasia. Quantitative image processing techniques and objective classification algorithms were also used to help aid in classifying measurement sites in human epithelium as neoplastic or non-neoplastic, a clinically important distinction.

Initial study presented in Chapter 3 evaluated the ability of the high-resolution microendoscope (HRME) to identify cervical neoplasia in patients at the women's clinic at Princess Marina Hospital in Botswana. Images were acquired from 52 sites in 26 patients. The images acquired by the microendoscope were assessed by both visual inspection by two expert observers and quantitative analysis to discriminate neoplastic (\geq CIN 2) from non-neoplastic cervical tissue. Results were compared to histopathology as the reference standard. Qualitative diagnoses by the expert HRME observers were compared with histopathologic diagnosis to calculate sensitivity and specificity. Observer #1 classified the images with a sensitivity and specificity of 86% and 70% respectively. Observer #2 classified the images with a sensitivity and specificity of 93% and 73% respectively. Quantitative analysis focused on assessment of nuclear size, since changes in nuclear size and nuclear-to-cytoplasmic (N/C) ratio are hallmark histopathologic features of cervical precancer. The sensitivity and specificity performance for this feature was 86% and 87%, respectively. For comparison, the sensitivity and specificity of clinical colposcopic impression for the same sites were 64% and 83%, respectively. Chapter 4 presents HRME validation results. The goal of this study was to test the reliability and reproducibility of the

results previously acquired using the same system and the same algorithm in the same low-resource setting. A total of 128 sites from 60 subjects were imaged; HRME images from each measured site were analyzed quantitatively using the same image analysis procedure to discriminate neoplastic (HGSIL or cancer) from non-neoplastic tissue (normal/benign or LGSIL). Results were compared to the gold standard of histopathology. High sensitivity of 90% and specificity 85% were reported in this study. These results are comparable to those previously reported.

Chapter 5 presents a portable, less complex, battery-powered, and robust wide-field system capable of operating in both fluorescence and reflectance. The performance of the multimodal optical imager (MDI) was measured, including using a USAF resolution target to verify that the MDI could resolve 88.3 micron lines. The feasibility of using this optical system in low-resource areas was also determined; the MDI was tested in Botswana as a pilot clinical study. In vivo MDI images were acquired from 60 unique sites in 30 patients. Computer-aided image analysis is also presented and its diagnostic performance reported. In low-resource areas where highly trained clinicians may not be available, automated algorithms to distinguish precancer from normal are very important to help healthcare providers with the diagnosis. Results were compared to the gold standard of histopathology. Relative red pixel intensity in the post acetic acid images and mean pixel intensity of hue channel in post Lugol's iodine images were found to be the two best performing features. The mean intensity of relative red for each measured site correctly classified non-neoplastic (normal/benign or low grade dysplasia) and neoplastic (high grade dysplasia) sites with a sensitivity of 86% and specificity of 71%, while the mean pixel intensity of hue channel correctly classified these measured sites into the same categories as described for mean intensity of relative red with a sensitivity of 86% and specificity

of 51%. A diagnostic algorithm that combines these two parameters was developed, and yielded a sensitivity of 86% and specificity of 74%. A combination of these features improved the specificity of each individual feature when used alone. For comparison, the sensitivity and specificity of clinical impression for the same sites were 57% and 84%, respectively.

Chapter 6 presents combination wide-field imaging with high-resolution optical imaging of the cervix. A total 118 sites in 63 patients were analyzed using the features described in Chapters 3, 4 and 5. A two-class linear discriminant algorithm was developed using the features from the post-acetic acid and post-Lugol's images. The hue intensity value of the post-Lugol's images for each measured site was found to be the single best performing feature. Sites determined to be positive by wide-field imaging were then evaluated by high-resolution imaging. Sites determined to be negative by wide-field imaging were considered to be negative for the combined analysis and were not further evaluated. A sensitivity of 82% and specificity of 85% were reported. The results suggest that the combination of these techniques can assist in the detection of cervical neoplasia and that these techniques can be implemented effectively in a low-resource setting.

There are several future research directions which could further assist clinicians in low resource settings to detect and treat cervical neoplasia.

Firstly, more research is needed to characterize images acquired from endocervical tissue. All data was taken from the transformation zone, however a few were reported to contain normal columnar epithelium by pathology. HRME images of these sites demonstrated higher N/C ratio and this might be a potential limitation of our high-resolution imaging.

More work needs to be done to optimize all the imaging modalities of the wide-field systems. In this work only cross-polarized white light imaging was used. Narrowband reflectance, and/or fluorescence imaging modes might improve sensitivity and specificity, by reducing specular glare, enhancing vascular contrast, and detecting alterations in tissue fluorescence associated with the presence of disease. Continuing development of classification algorithms for both wide-field and high-resolution systems could potentially provide a way to bridge the gap of cervical cancer screening for developing countries

Building systems independent of a computer/Laptop can further reduce the cost and complexity of optical systems used in this dissertation. The cost of cellphones has dramatically gone down over the few years due to massive volume of wireless communication in the world. Hardware and software capabilities of cellphones have greatly advanced leading to utilization in medical imaging. A great opportunity exists in developing cellphone-based imaging systems. This can potentially make an impact in developing countries, where most of the cellphone usage has been reported. I propose the next be to convert the MDI and HRME into cellphone-based platforms. This will not only greatly reduced the cost associated with the devices but can improve telemedicine in these areas. That is, a less experienced health provider in a rural area may easily send images to a more experienced clinician in the city by just a click of a button for quick consultation, without the need of a computer and reliable Internet connection.

REFERENCES

1. Jemal A, Bray F, Center MM, Ferlay J, Ward E, et al. (2011) Global cancer statistics. *CA Cancer J Clin* 61: 69–90
2. Parkin, D.M., Bray, F., Ferlay, J. & Pisani, P. Global cancer statistics, 2002. *CA Cancer J Clin* **55**, 74-108 (2005).
3. Parkin DM, Bray F. Chapter 2: the burden of HPV-related cancers. *Vaccine* 2006;24: Suppl 3:S11-S25.
4. Ministry of Health, Botswana (2008).
5. Mandelblatt, J.S., Kanetsky, P., Eggert, L. & Gold, K. Is HIV infection a cofactor for cervical squamous cell neoplasia? *Cancer Epidemiol Biomarkers Prev* **8**, 97-106 (1999).
6. L G Koss, “The Papanicolaou test for cervical cancer detection: a triumph and a tragedy,” *J Am Med Assoc* 261; 737-743 (1989)
7. S J Goldie, et al. “Cost-effectiveness of cervical-cancer screening in five developing countries,” *N. Engl. J. Med.* 353; 2158–2168 (2005).
8. M F Mitchell, D Schottenfeld, G Tortolero-Luna, S B Cantor, R Richards-Kortum, “Colposcopy for the diagnosis of squamous intraepithelial lesions: a metaanalysis,” *Obstet. Gynecol.* 91; 626–631 (1998)
9. Indman, P. *Advanced Gynecology Solution* ;
http://www.gynalternatives.com/cervix_structure.htm (accessed on 03/02/13)
10. Kurman, R. J. **Blaustein's Pathology of the Female Genital Tract (4th Ed)**;
Springer- Verlag: New York, NY, 1994.
11. Anderson M, Jordan J, Morse A, Sharp F. **A text and atlas of integrated colposcopy**;
January 1991.
12. Silverthorn, D. *Human Physiology: An Integrated Approach (2nd Ed.)*; Prentice Hall:
Upper Saddle River, NJ, 2001.
13. A. Blaustein and R.J Kurman, **Blaustein's Pathology of the Female Genital Tract**,
Springer, New York (2002).

14. C. P. Crum, **Diagnostic Gynecologic and Obstetrics Pathology**, Elsevier Saunders, Philadelphia (2006).
15. V. Kumur et al, **Robbins and Cotran Pathologic Basis of Disease**, Elsevier Saunders, Philadelphia (2005).
16. Kalof A N, Cooper K J, **Our approach to squamous intraepithelial lesions of the uterine cervix**, Clin Pathol 2007;60:449-455.
17. Indman, P. Advanced Gynecology Solution ;
http://www.gynalternatives.com/cervix_structure.htm (accessed on 03/02/13)
18. http://www.cancer.org/docroot/CRI/content/CRI_2_4_1X_what_is_cervical_cancer_8.asp (accessed on 03/02/13)
19. M F Mitchell, "Preinvasive diseases of the female low genital track," in Operative Gynecology, D M Greshenson, A DeCherney, S Curry, eds. (Saunders, Philadelphia, 1993), p. 231.
20. R J Kurman, D E Herison, A L Herbst, K L Noller, M H Schiffman, "Interim guidelines for management of abnormal cervical cytology," J Am Med Assoc 271; 1866-1869 (1994)
21. Mitchell, M. F.; Cantor, S. B.; Brookner, C.; Utzinger, U.; Schottenfeld, Richards-Kortum, R. Obstetrics & Gynecology **1999**, 94, 889.
22. S B Cantor, M Follen-Mitchell, G Tortolero-Luna, C Bratka, D Bodurka, R Richards-Kortum, "Costeffectiveness analysis of diagnosis and management of cervical squamous intraepithelial lesions," Obstet Gynecol 91; 270-277 (1998)
23. Walboomers, J. M. et al. Human papillomavirus is a necessary cause of invasive cervical cancer worldwide. J. Pathol. **189**, 12–19 (1999).
24. Lungu O, Sun XW, Wright TC, et al. A polymerase chain reaction– enzyme-linked immunosorbent assay method for detecting human papillomavirus in cervical carcinoma and high grade cervical cancer precursors. Obstet Gynecol 1995;85:337-42.

25. Gitsch G, Reinthaller A, Tatra G, et al. Diagnosis of cervical intraepithelial neoplasia and human papillomavirus infection: punch biopsy versus cervical smear. *Arch Gynecol Obstet* 1991; 249:179-84.
26. Munoz N, Bosch FX, de Sanjose S, et al. Epidemiologic classification of human papillomavirus types associated with cervical cancer. *N Engl Med* 2003;348:518-527.
27. Bosch FX, Manos MM, Munoz N, et al. Prevalence of human papillomavirus in cervical cancer: a worldwide perspective. International biological study on cervical cancer (IBSCC) Study Group. *J Natl Cancer Inst* 1995; 87:796-802.
28. Cohen, J. Public health. High hopes and dilemmas for a cervical cancer vaccine. *Science* **308**, 618–621 (2005).
29. Jan M. Agosti, and Sue J. Goldie. Introducing HPV Vaccine in Developing Countries —Key Challenges and Issues. *N. Engl . J. Med* 356; 19 (2007).
30. Agosti, J. M. & Goldie, S. J. Introducing HPV vaccine in developing countries — key challenges and issues. *N. Engl. J. Med.* **356**, 1908–1910 (2007).
31. Jeronimo, J. et al. Visual inspection with acetic acid for cervical cancer screening outside of low-resource settings. *Rev. Panam. Salud Publica* **17**, 1–5 (2005).
32. Cuzick J, Szarewski A, Terry G, et al. Human papilloma virus testing in primary cervical screening. *Lancet* 1995; 345:1533-6.
33. Reid R, Lorincz AT. Human papillomavirus tests. *Baillieres Clin Obstet Gynecol* 1995;9:65-103.
34. Louise Kuhn. et al. Human Paillomavirus DNA Testing for Cervical Cancer Screening in Low-Resource Settings. *J. NCI.* 92-10 (2000)
35. Qiao YL, Sellors JW, Eder PS, Bao YP, Lim JM, et al. (2008) A new HPV-DNA test for cervical-cancer screening in developing regions: a cross-sectional study of clinical accuracy in rural China. *Lancet Oncol* 9: 929–936.

36. Sankaranarayanan, R. et al. Visual inspection of the uterine cervix after the application of acetic acid in the detection of cervical carcinoma and its precursors. *Cancer* **83**, 2150–2156 (1998).
37. Sankaranarayanan, R. et al. Effect of visual screening on cervical cancer incidence and mortality in Tamil Nadu, India: a cluster-randomised trial. *Lancet* **370**, 398–406 (2007).
38. Denny, L., Kuhn, L., Pollack, A. & Wright, T. C. Jr. Direct visual inspection for cervical cancer screening: an analysis of factors influencing test performance. *Cancer* **94**, 1699–1707 (2002).
39. Visual inspection with acetic acid for cervical-cancer screening: test qualities in a primary-care setting. University of Zimbabwe/JHPIEGO Cervical Cancer Project. *Lancet* **353**, 869–873 (1999).
40. Denny, L., Kuhn, L., Pollack, A., Wainwright, H. & Wright, T. C. Jr. Evaluation of alternative methods of cervical cancer screening for resource-poor settings. *Cancer* **89**, 826–833 (2000).
41. Belinson, J. L. et al. Cervical cancer screening by simple visual inspection after acetic acid. *Obstet. Gynecol.* **98**, 441–444 (2001).
42. Cronje, H. S. et al. A comparison of four screening methods for cervical neoplasia in a developing country. *Am. J. Obstet. Gynecol.* **188**, 395–400 (2003).
43. Sankaranarayanan, R. et al. Accuracy of visual screening for cervical neoplasia: Results from an IARC multicentre study in India and Africa. *Int. J. Cancer* **110**, 907–913 (2004).
44. M C Pierce, D J Javier, R Richards-Kortum, “Optical contrast agents and imaging systems for detection and diagnosis of cancer,” *Int J Cancer* 123; 1979-1990 (2008).
45. R A Drezek et al. “Laser scanning confocal microscopy of cervical tissue before and after application of acetic acid,” *Amer. J. Obstet. Gynecol.* 182; 1135–1139 (2000)

46. M C Skala et al. "Multiphoton microscopy of endogenous fluorescence differentiates normal, precancerous, and cancerous squamous epithelial tissues," *Cancer Res.* 65; 1180–1186 (2005)
47. R S DaCosta, B C Wilson, N E Marcon, "Fluorescence and spectral imaging," *Scientific World Journal* 7; 2046–2071 (2007)
48. L T Perelman, "Optical diagnostic technology based on light scattering spectroscopy for early cancer detection," *Expert Rev. Med. Devices* 3; 787–803 (2006)
49. N Ramanujam, "Fluorescence spectroscopy of neoplastic and non-neoplastic tissues," *Neoplasia* 2; 89–117 (2000)
50. Mourant, J. R., Canpolat, M., Brocker, C., Esponda-Ramos, O., Johnson, T. M., Matanock, A., Stetter, K., Freyer, J. P. *Journal of Biomedical Optics* **2000**, 5, 131.
51. Drezek, R. et al. Light scattering from cervical cells throughout neoplastic progression: influence of nuclear morphology, DNA content, and chromatin texture. *J. Biomed. Opt.* **8**, 7–16 (2003).
52. Arifler, D. et al. Light scattering from normal and dysplastic cervical cells at different epithelial depths: finite-difference time-domain modeling with a perfectly matched layer boundary condition. *J. Biomed. Opt.* **8**, 484–494 (2003).
53. RALPH S DACOSTA. et al. New optical technologies for earlier endoscopic diagnosis of premalignant gastrointestinal lesions. *Journal of Gastroenterology and Hepatology* (2002) **17** (Suppl.) S85–S104.
54. Zuluaga, A. F. et al. Contrast agents for confocal microscopy: how simple chemicals affect confocal images of normal and cancer cells in suspension. *J. Biomed. Opt.* **7**, 398–403 (2002).
55. Collier, T., Follen, M., Malpica, A. & Richards-Kortum, R. Sources of scattering in cervical tissue: determination of the scattering coefficient by confocal microscopy. *Appl. Opt.* **44**, 2072–2081 (2005).

56. Collier, T., Guillaud, M., Follen, M., Malpica, A. & Richards-Kortum, R. Real-time reflectance confocal microscopy: comparison of two-dimensional images and three-dimensional image stacks for detection of cervical precancer. *J. Biomed. Opt.* **12**, 024021 (2007).
57. Dellas, A., Moch, H., Schultheiss, E., Feichter, G., Almendra, A. C., Gudat, F., Torhorst, Journal of Gynecologic Oncology **1997**, 67, 27.
58. Richards-Kortum, R.; Sevick-Muraca, E. *Annual Review of Physical Chemistry* **1996**, 47, 555.
59. Pavlova, I. et al. Microanatomical and biochemical origins of normal and precancerous cervical autofluorescence using laser-scanning fluorescence confocal microscopy. *Photochem. Photobiol.* **77**, 550–555 (2003).
60. Drezek, R. et al. Autofluorescence microscopy of fresh cervical-tissue sections reveals alterations in tissue biochemistry with dysplasia. *Photochem. Photobiol.* **73**, 636–641 (2001).
61. Lohmann, W., Mussmann, J., Lohmann, C. & Kunzel, W. Native fluorescence of unstained cryo-sections of the cervix uteri compared with histological observations. *Naturwissenschaften* **76**, 125–127 (1989).
62. J M Benavides, S Chang, S Y Park, R Richards-Kortum, N MacKinnon, C MacCaulay, A Milbourne, A Malpica, M Follen, “Multispectral digital colposcopy for in vivo detection of cervical cancer,” *Opt Express* 11; 1223-1236 (2003)
63. S Y Park, M Follen, A Milbourne, H Rhodes, A Malpica, N MacKinnon, C MacAulay, M K Markey, R Richards-Kortum, “Automated image analysis of digital colposcopy for the detection of cervical neoplasia,” *J Biomed Opt* 13; 014029 (2008).
64. Huh, W. K. et al. Optical detection of high-grade cervical intraepithelial neoplasia in vivo: results of a 604-patient study. *Am. J. Obstet. Gynecol.* **190**, 1249–1257 (2004).
65. Alvarez, R. D. & Wright, T. C. Effective cervical neoplasia detection with a novel optical detection system: a randomized trial. *Gynecol. Oncol.* **104**, 281–289 (2007).

66. Ferris, D. G. et al. Multimodal hyperspectral imaging for the noninvasive diagnosis of cervical neoplasia. *J. Low. Genit. Tract Dis.* **5**, 65–72 (2001).
67. DeSantis, T. et al. Spectroscopic imaging as a triage test for cervical disease: a prospective multicenter clinical trial. *J. Low. Genit. Tract Dis.* **11**, 18–24 (2007).
68. Orfanoudaki, I. M. et al. A clinical study of optical biopsy of the uterine cervix using a multispectral imaging system. *Gynecol. Oncol.* **96**, 119–131 (2005).
69. Milbourne, A. et al. Results of a pilot study of multispectral digital colposcopy for the in vivo detection of cervical intraepithelial neoplasia. *Gynecol. Oncol.* **99**, S67–75 (2005).
70. Alvarez, R. D. & Wright, T. C. Jr. Increased detection of high-grade cervical intraepithelial neoplasia utilizing an optical detection system as an adjunct to colposcopy. *Gynecol. Oncol.* **106**, 23–28 (2007).
71. D Roblyer, R Richards-Kortum, K Sokolov, A K El-Naggar, M D Williams, C Kurachi, A M Gillenwater, “Multispectral optical imaging device for in vivo detection of oral neoplasia,” *J Biomed Opt* 13; 024019 (2008).
72. D Roblyer, C Kurachi, V Stepanek, M D Williams, A K El-Naggar, J J Lee, A M Gillenwater, R Richards-Kortum, “Objective detection and delineation of oral neoplasia using autofluorescence imaging,” *Cancer Prevention Research*; 2(5):423-31, 2009. PMID: 19401530.
73. M Rahman, P Chaturvedi, A M Gillenwater, R Richards-Kortum, “Low-cost, multimodal, portable screening system for early detection of oral cancer,” *J Biomed Opt* 13; 030502 (2008).
74. Mohammed S. Rahman, Nilesh Ingole, Darren Roblyer, Vanda Stepanek, Rebecca Richards-Kortum, Ann Gillenwater, Surendra Shastri, and Pankaj Chaturvedi; Evaluation of A Low-Cost, Portable Imaging System for Early Detection of Oral Cancer, *Head & Neck Oncology*, 2:10, 2010, doi:10.1186/1758-3284-2-10.
75. T Collier, A Lacy, R Richards-Kortum, A Malpica, M Follen, “Near real-time confocal microscopy of amelanotic tissue: detection of dysplasia in ex vivo cervical tissue,” *Acad Radiol* 9; 504-12 (2002)

76. N Thekkek, R Richards-Kortum, "Optical imaging for cervical cancer detection: solutions for a continuing global problem" *Nat Rev Cancer* 8; 725-731 (2008)
77. Evans, J. A. & Nishioka, N. S. Endoscopic confocal microscopy. *Curr. Opin. Gastroenterol.* **21**, 5578–584 (2005).
78. Conchello, J.A. and J.W. Lichtman, Optical sectioning microscopy. *Nat Methods*, 2005. **2**(12): p. 920-31.
79. Tan, J., et al., Detection of cervical intraepithelial neoplasia in vivo using confocal endomicroscopy. *Gynecologic Oncology* **2009**, 116:1663-1670.
80. Kiesslich, R., et al., Diagnosing *Helicobacter pylori* in vivo by confocal laser endoscopy. *Gastroenterology*, 2005. **128**(7): p. 2119-23.
81. Beechey-Newman, N., et al., Breast duct microendoscopy in nipple discharge: microbrush improves cytology. *Surg Endosc*, 2005. **19**(12): p. 1648-51.
82. Jung, J.C., et al., In vivo mammalian brain imaging using one- and two-photon fluorescence microendoscopy. *J Neurophysiol*, 2004. **92**(5): p. 3121-33.
83. Hirano, M., Y. Yamashita, and A. Miyakawa, In vivo visualization of hippocampal cells and dynamics of Ca²⁺ concentration during anoxia: feasibility of a fiber-optic plate microscope system for in vivo experiments. *Brain Res*, 1996. **732**(1-2): p. 61-8.
84. Monfared, A., et al., In vivo imaging of mammalian cochlear blood flow using fluorescence microendoscopy. *Otol Neurotol*, 2006. **27**(2): p. 144-52.
85. Levene, M.J., et al., In vivo multiphoton microscopy of deep brain tissue. *J Neurophysiol*, 2004. **91**(4): p. 1908-12.
86. Poe, G.R., D.M. Rector, and R.M. Harper, Hippocampal reflected optical patterns during sleep and waking states in the freely behaving cat. *J Neurosci*, 1994. **14**(5 Pt 2): p. 2933-42.
87. Kiesslich, R., et al., Confocal laser endoscopy for diagnosing intraepithelial neoplasias and colorectal cancer in vivo. *Gastroenterology*, 2004. **127**(3): p. 706-13.

88. T J Muldoon, M C Pierce, D L Nida, M D Williams, A Gillenwater, R Richards-Kortum, "Subcellular resolution molecular imaging within living tissue by fiber microendoscopy" *Opt Express* 15; 16413-16423 (2007)
89. T J Muldoon, S Anandasabapathy, D Maru, R Richards-Kortum, "High-resolution imaging in Barrett's esophagus: a novel, low-cost endoscopic microscope," *Gastrointest Endosc* 68; 737- 744 (2008)
90. Mehmet, A., Electrochemical and Spectroscopic Studies of the Interaction of Proflavine with DNA. *Analytical Sciences* 22, 439-443 (2006).
91. <http://omlc.ogi.edu/spectra/PhotochemCAD/html/proflavin> (pH7).html. Accessed on October 10, 2010.
92. Russell, D. S. and Falconer, M. A. Antiseptics in brain wounds; experimental study of histological reaction of cerebral tissue to various antiseptic solutions. *British Journal of Surgery* 28, 472-99.
93. Rubbo, S. D. (1947). The influence of chemical constitution on toxicity. I. A general survey of the acidine series. *British Journal of Experimental Pathology* 28, 1-11.
94. Gorrod, L. P. (1940). Action of Antiseptics on wounds. *Lancet* I, 798-9.
95. Cancer IAFRo (2005) Cervix Cancer Screening. In: Organization WH, editor. *Handbook of Cancer Prevention*. Lyon, France: IARC Press.
96. Sankaranarayanan R, Nene BM, Shastri SS, Jayant K, Muwonge R, et al. (2009) HPV screening for cervical cancer in rural India. *N Engl J Med* 360: 1385–1394.
97. Sankaranarayanan R, Nessa A, Esmey PO, Dangou JM (2012) Visual inspection methods for cervical cancer prevention. *Best Pract Res Clin Obstet Gynaecol* 26:221–232.
98. Polglase AL, McLaren WJ, Skinner SA, Kiesslich R, Neurath MF, et al. (2005) A fluorescence confocal endomicroscope for in vivo microscopy of the upper- and the lower-GI tract. *Gastrointest Endosc* 62: 686–695.

99. Muldoon TJ, Roblyer D, Williams MD, Stepanek VM, Richards-Kortum R, et al. (2012) Noninvasive imaging of oral neoplasia with a high-resolution fiberoptic microendoscope. *Head Neck* 34: 305–312.
100. Vila PM, Thekkekk N, Richards-Kortum R, Anandasabapathy S (2011) Use of in vivo real-time optical imaging for esophageal neoplasia. *Mt Sinai J Med* 78:894–904.
101. Pierce MC, Schwarz RA, Bhattar VS, Mondrik S, Williams MD, et al. (2012) Accuracy of In Vivo Multimodal Optical Imaging for Detection of Oral Neoplasia. *Cancer Prev Res (Phila)*.
102. Pierce M, Yu D, Richards-Kortum R (2011) High-resolution fiber-optic microendoscopy for in situ cellular imaging. *J Vis Exp*.
103. Sellors JW, Sankaranarayanan R (2003) Colposcopy and Treatment of Cervical Intraepithelial Neoplasia: A Beginner's Manual: International Agency for Research on Cancer.
104. Baak I, Stoler M, Anderson M, Robboy S (2009) Cervical precancer (intraepithelial neoplasia), including biomarkers and colposcopy. In: Robboy S, Mutter G, Prat J, Bentley R, Rissel P, et al., editors. *Robboy's Pathology of the Female Reproductive Tract*. 2nd Edition ed: Churchill Livingstone Elsevier. pp. 189–226.
105. World Health Organization World Health Organization Department of Reproductive Health and Research and Department of Chronic Diseases and Health Promotion (2006) *Comprehensive cervical cancer control: A guide to essential practice*.
106. Maiman M, Fruchter RG, Serur E, Remy JC, Feuer G, et al. (1990) Human immunodeficiency virus infection and cervical neoplasia. *Gynecol Oncol* 38: 377–382.

107. Sauvaget C, Fayette JM, Muwonge R, Wesley R, Sankaranarayanan R (2011) Accuracy of visual inspection with acetic acid for cervical cancer screening. *Int J Gynaecol Obstet* 113: 14–24.
108. Ramogola-Masire D, de Klerk R, Monare B, Ratshaa B, Friedman HM, et al. (2012) Cervical cancer prevention in HIV-infected women using the “see and treat” approach in Botswana. *J Acquir Immune Defic Syndr* 59: 308–313.
109. American Cancer Society , Cervical Cancer: Prevention and Early Detection, <http://www.cancer.org/Cancer/CervicalCancer/MoreInformation/CervicalCancerPreventionandEarlyDetection/cervical-cancer-prevention-and-early-detection-find-pre-cancer-changes> (accessed on January 22, 2012)
110. Denny L et al. Screen-and-treat approaches for cervical cancer prevention in low-resource settings: a randomized controlled trial. *Journal of the American Medical Association*. 2005; 294 (17):2173-2181.
111. Quinn MK, Bubi TC, Pierce MC, Kayembe MK, Ramogola-Masire D, et al. (2012) High-Resolution Microendoscopy for the Detection of Cervical Neoplasia in Low-Resource Settings. *PLoS ONE* 7(9): e44924. doi:10.1371/journal.pone.0044924
112. Rosbach KJ, Shin D, Muldoon TJ et al, “High-resolution fiber optic microscopy with fluorescence contrast enhancement for identification of axillary lymph node metastases in breast cancer: a pilot study. *J Biomed Opt Express* 2010; 1:911-922.
113. Mathew A, George PS. Trends in incidence and mortality rates of squamous cell carcinoma and adenocarcinoma of cervix–worldwide. *Asian Pac J Cancer Prev*. 2009; 10:645-650.
114. Vizcaino AP, Moreno V, Bosch FX, et al. International trends in incidence of cervical cancer: II. Squamous-cell carcinoma. *Int J Cancer*. 2000; 86:429-435.
115. Sankaranarayanan, R. et al. A critical assessment of screening methods for cervical neoplasia. doi:10.1016/j.ijgo.2005.01.009.
116. Ji, Q., Engel, J. & Craine, E. Texture analysis for classification of cervix lesions. *IEEE Trans Med Imaging* **19**, 1144-9 (2000).

117. B. W. Pogue, H. B. Kaufman, A. Zelenchuk, W. Harper, G. C. Burke, E. E. Burke, and D. M. Harper, "Analysis of acetic acid-induced whitening of high-grade squamous intraepithelial lesions," *J. Biomed. Opt.* **6**, 397–403 (2001).
118. C. Balas, "A novel optical imaging method for the early detection, quantitative grading, and mapping of cancerous and precancerous lesions of cervix," *IEEE Trans. Biomed. Eng.* **48**, 96.104 (2001).
119. B. W. Pogue, M. A. Mycek, and D. Harper, "Image analysis for discrimination of cervical neoplasia" *Journal of Biomedical Optics*. January 2000. Vol. 5 No. 1.
120. Sankaranarayanan, R., et al., Effect of visual screening on cervical cancer incidence and mortality in Tamil Nadu, India: a cluster-randomised trial. *Lancet*, 2007. **370**(9585): p. 398-406.
121. Visual inspection with acetic acid for cervical-cancer screening: test qualities in a primary-care setting. University of Zimbabwe/JHPIEGO Cervical Cancer Project. *Lancet*, 1999. **353**(9156): p. 869-73.
122. Belinson SE, Belinson JL (2010). Human papillomavirus DNA testing for cervical cancer screening: practical aspects in developing countries. *Mol Diagn Ther*, **14**, 215-22.